CLIMATE SENSITIVITY: ANALYSIS OF FEEDBACK MECHANISMS

J. Hansen, A. Lacis, D. Rind, G. Russell

NASA/Goddard Space Flight Center, Institute for Space Studies
2880 Broadway, New York, NY 10025

P. Stone

Center for Meteorology and Physical Oceanography
Massachusetts Institute of Technology, Cambridge, MA 02139

I. Fung

Lamont-Doherty Geological Observatory of Columbia University
Palisades, NY 10964

R. Ruedy, J. Lerner

M/A COM Sigma Data, Inc.
2880 Broadway, New York, NY 10025

Abstract. We study climate sensitivity and feedback processes in three independent ways: (1) by using a three dimensional (3-D) global climate model for experiments in which solar irradiance S_o is increased 2 percent or CO_2 is doubled, (2) by using the CLIMAP climate boundary conditions to analyze the contributions of different physical processes to the cooling of the last ice age (18K years ago), and (3) by using estimated changes in global temperature and the abundance of atmospheric greenhouse gases to deduce an empirical climate sensitivity for the period 1850-1980.

Our 3-D global climate model yields a warming of ~4°C for either a 2 percent increase of S_o or doubled CO_2. This indicates a net feedback factor of f = 3-4, because either of these forcings would cause the earth's surface temperature to warm 1.2-1.3°C to restore radiative balance with space, if other factors remained unchanged. Principal positive feedback processes in the model are changes in atmospheric water vapor, clouds and snow/ice cover. Feedback factors calculated for these processes, with atmospheric dynamical feedbacks implicitly incorporated, are respectively $f_{water\ vapor} \sim 1.6$, $f_{clouds} \sim 1.3$ and $f_{snow/ice} \sim 1.1$, with the latter mainly caused by sea ice changes. A number of potential feedbacks, such as land ice cover, vegetation cover and ocean heat transport were held fixed in these experiments.

We calculate land ice, sea ice and vegetation feedbacks for the 18K climate to be $f_{land\ ice} \sim 1.2\text{-}1.3$, $f_{sea\ ice} \sim 1.2$, and $f_{vegetation} \sim 1.05\text{-}1.1$ from their effect on the radiation budget at the top of the atmosphere. This sea ice feedback at 18K is consistent with the smaller $f_{snow/ice} \sim 1.1$ in the S_o and CO_2 experiments, which applied to a warmer earth with less sea ice. We also obtain an empirical estimate of f = 2-4 for the fast feedback processes (water vapor, clouds, sea ice) operating on 10-100 year time scales by comparing the cooling due to slow or specified changes (land ice, CO_2, vegetation) to the total cooling at 18K.

The temperature increase believed to have occurred in the past 130 years (approximately 0.5°C) is also found to imply a climate sensitivity of 2.5-5°C for doubled CO_2 (f = 2-4), if (1) the temperature increase is due to the added greenhouse gases, (2) the 1850 CO_2 abundance was 270±10 ppm, and (3) the heat perturbation is mixed like a passive tracer in the ocean with vertical mixing coefficient $k \sim 1\ cm^2\ s^{-1}$.

These analyses indicate that f is substantially greater than unity on all time scales. Our best estimate for the current climate due to processes operating on the 10-100 year time scale is f = 2-4, corresponding to a climate sensitivity of 2.5-5°C for doubled CO_2. The physical process contributing the greatest uncertainty to f on this time scale appears to be the cloud feedback.

We show that the ocean's thermal relaxation time depends strongly on f. The e-folding time

constant for response of the isolated ocean mixed layer is about 15 years, for the estimated value of f. This time is sufficiently long to allow substantial heat exchange between the mixed layer and deeper layers. For f = 3-4 the response time of the surface temperature to a heating perturbation is of order 100 years, if the perturbation is sufficiently small that it does not alter the rate of heat exchange with the deeper ocean.

The climate sensitivity we have inferred is larger than that stated in the Carbon Dioxide Assessment Committee report (CDAC, 1983). Their result is based on the empirical temperature increase in the past 130 years, but their analysis did not account for the dependence of the ocean response time on climate sensitivity. Their choice of a fixed 15 year response time biased their result to low sensitivities.

We infer that, because of recent increases in atmospheric CO_2 and trace gases, there is a large, rapidly growing gap between current climate and the equilibrium climate for current atmospheric composition. Based on the climate sensitivity we have estimated, the amount of greenhouse gases presently in the atmosphere will cause an eventual global mean warming of about 1°C, making the global temperature at least comparable to that of the Altithermal, the warmest period in the past 100,000 years. Projection of future climate trends on the 10-100 year time scale depends crucially upon improved understanding of ocean dynamics, particularly upon how ocean mixing will respond to climate change at the ocean surface.

Introduction

Over a sufficient length of time, discussed below, thermal radiation from the earth must balance absorbed solar radiation. This energy balance requirement defines the effective radiating temperature of the earth, T_e, from

$$\pi R^2(1 - A)S_0 = 4\pi R^2\sigma T_e^4 \qquad (1)$$

or

$$T_e = [S_0(1 - A)/4\sigma]^{1/4} = (s/\sigma)^{1/4} \qquad (2)$$

where R is the earth radius, A the earth albedo, S_0 the solar irradiance, s the mean flux of absorbed solar radiation per unit area and σ the Stefan-Boltzmann constant. Since A ~ 0.3 and S_0 ~ 1367 W m^{-2}, s ~ 239 W m^{-2} and this requirement of energy balance yields T_e ~ 255K. The effective radiating temperature is also the physical temperature at an appropriately defined mean level of emission to space. In the earth's atmosphere this mean level of emission to space is at altitude H ~ 6 km. Since the mean tropospheric temperature gradient is ~5.5°C km^{-1}, the surface temperature is T ~ 288K, ~33K warmer than T_e.

It is apparent from (2) that for changes of solar irradiance

$$\frac{dT_e}{T_e} = \frac{1}{4}\frac{dS_0}{S_0} = \frac{1}{4}\frac{ds}{s} \quad . \qquad (3)$$

Thus if S_0 increases by a small percentage δ, T_e increases by $\delta/4$. For example, a 2 percent change in solar irradiance would change T_e by about 0.5 percent, or 1.2-1.3°C. If the atmospheric temperature structure and all other factors remained fixed, the surface temperature would increase by the same amount as T_e. Of course all factors are not fixed, and we therefore define the net feedback factor, f, by

$$\Delta T_{eq} = f\,\Delta T_0 \qquad (4)$$

where ΔT_{eq} is the equilibrium change of global mean surface air temperature and ΔT_0 is the change of surface temperature that would be required to restore radiative equilibrium if no feedbacks occurred.

We use procedures and terminology of feedback studies in electronics (Bode, 1945) to help analyze the contributions of different feedback processes. We define the system gain as the ratio of the net feedback portion of the temperature change to the total temperature change

$$g = \frac{\Delta T_{feedbacks}}{\Delta T_{eq}} \quad . \qquad (5)$$

Since

$$\Delta T_{eq} = \Delta T_0 + \Delta T_{feedbacks}, \qquad (6)$$

it follows that the relation between the feedback factor and gain is

$$f = \frac{1}{1 - g} \quad . \qquad (7)$$

In general a number of physical processes contribute to f, and it is common to associate a feedback factor f_i with a given process i, where f_i is the feedback factor which would exist if all other feedbacks were inoperative. If it is assumed that the feedbacks are independent, feedback contributions to the temperature change can be separated into portions identifiable with individual feedbacks,

$$\Delta T_{feedbacks} = \sum_i \Delta T_i, \qquad (8)$$

with

$$g = \sum_i \frac{\Delta T_i}{\Delta T_{eq}} = \sum_i g_i \qquad (9)$$

and

$$\Delta T_{eq} = \frac{1}{1 - \sum_i g_i} \Delta T_o \quad . \qquad (10)$$

It follows that two feedback gains combine linearly as

$$g = g_1 + g_2 \ , \qquad (11)$$

but the feedback factors combine as

$$f = \frac{f_1 f_2}{f_1 + f_2 - f_1 f_2} \quad . \qquad (12)$$

Thus even when feedback processes are linear and independent the feedback factors are not multiplicative. For example, a feedback process with gain $g_i = 1/3$ operating by itself would cause a 50 percent increase in ΔT_{eq} compared to the no feedback radiative response, i.e., $f_i = 1.5$. If a second feedback process of the same strength is also operating, the net feedback is $f = 3$ (not 2.25). One implication is that, if strong positive feedback exists, a moderate additional positive feedback may cause a large increase in the net feedback factor and thus in climate sensitivity.

The feedback factor f provides an intuitive quantification of the strength of feedbacks and a convenient way to describe the effect of feedbacks on the transient climate response. The gain g allows clear comparison of the contributions of different mechanisms to total climate change. The above formalism relates f and g and provides a framework for analyzing feedback interactions and climate sensitivity.

A number of physical mechanisms have been identified as causing significant climate feedback (Kellogg and Schneider, 1974). As examples, we mention two of these mechanisms here. Water vapor feedback arises from the ability of the atmosphere to hold more water vapor as temperature increases. The added water vapor increases the infrared opacity of the atmosphere, raising the mean level of infrared emission to space to greater altitude, where it is colder. Because the planetary radiation to space temporarily does not balance absorbed solar energy, the planet must warm to restore energy balance; thus $f_w > 1$ and $g_w > 0$, a condition described as a positive feedback. Ice/snow feedback is also positive; it operates by increasing the amount of solar energy absorbed by the planet as ice melts.

Feedback analyses will be most useful if the feedback factors are independent to first order of the nature of the radiative forcing (at the top of the atmosphere). The similar model responses we obtain in our S_o and CO_2 experiments tend to corroborate this possibility, although there are some significant differences in the feedbacks for solar and CO_2 forcings. We expect the strength of feedbacks to have some dependence on the initial climate state and thus on the magnitude of the climate forcing; for example, the ice/snow albedo feedback is expected to change with climate as the cryospheric region grows or shrinks.

We examine feedback processes quantitatively in the following sections by means of 3-D climate model simulations and analysis of conditions during the last ice age (18K years ago). The 3-D experiments include doubling CO_2 and increasing S_o by 2 percent, forcings of roughly equal magnitude which have also been employed by Manabe and Wetherald (1975) and Wetherald and Manabe (1975). 18K simulations with a 3-D general circulation model have previously been performed by Williams et al. (1974), Gates (1976) and Manabe and Hahn (1977).

Three-Dimensional Climate Model

The global climate model we employ is described and its abilities and limitations for simulating today's climate are documented as model II (Hansen et al., 1983b, hereafter referred to as paper 1). We note here only that the model solves the simultaneous equations for conservation of energy, momentum, mass and water and the equation of state on a coarse grid with horizontal resolution 8° latitude by 10° longitude and with 9 atmospheric layers. The radiation includes the radiatively significant atmospheric gases, aerosols and cloud particles. Cloud cover and height are computed. The diurnal and seasonal cycles are included. The ground hydrology and surface albedo depend upon the local vegetation. Snow depth is computed and snow albedo includes effects of snow age and masking by vegetation.

Ocean temperatures and ice cover are specified climatologically in the documented model II. In the experiments described here, ocean temperatures and ice cover are computed based on energy exchange with the atmosphere, ocean heat transport, and the ocean mixed layer heat capacity. The latter two are specified, but vary seasonally at each gridpoint. Monthly mixed layer depths are climatological, compiled from NODC mechanical bathythermograph data (NOAA, 1974) and from temperature and salinity profiles in the southern ocean (Gordon, 1982). The resulting global-mean seasonal-maximum mixed layer depth is 110m. In our 3-D experiments a 65m maximum is imposed on the mixed layer depth to minimize computer time; this yields a global-mean seasonal-maximum mixed layer depth of 63m. The 65m maximum depth is sufficient to make the mixed layer thermal response time much greater than one year and provide a realistic representation of seasonal temperature variations, so the mixed layer depth limitation should not significantly affect the modeled equilibrium climate.

The ocean heat transport was obtained from the divergence of heat implied by energy conservation at each ocean gridpoint in the documented

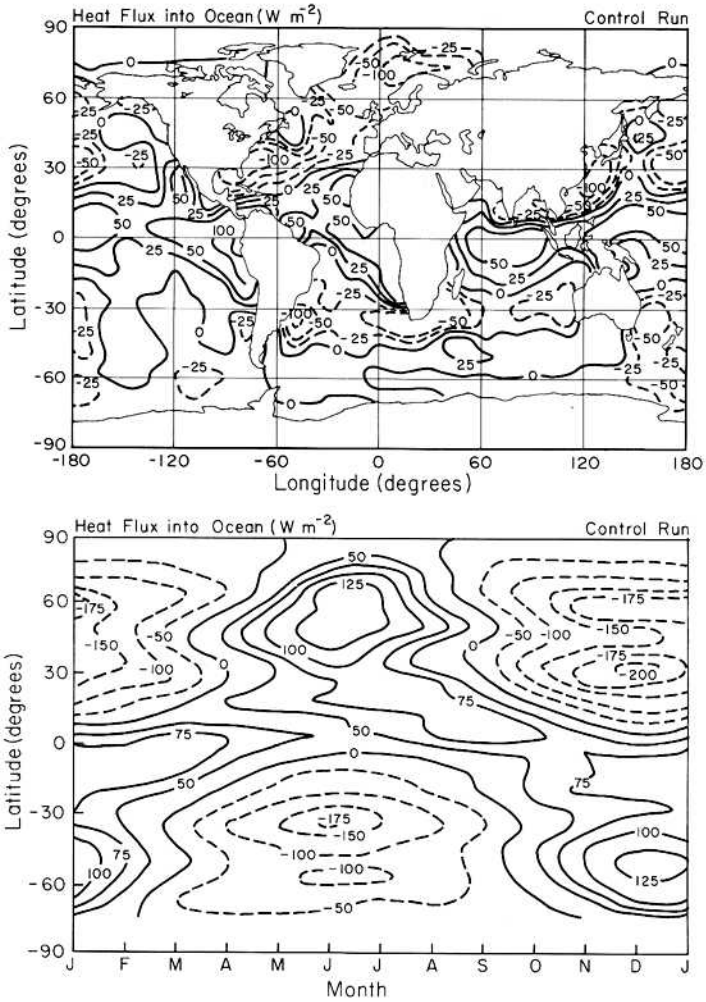

Fig. 1. Specified heat flux into the ocean surface in the 3-D climate model experiments, obtained from the model II run of paper 1 which had specified climatological seasonally-varying ocean surface temperature and ocean ice cover. (a) is the geographical distribution of the annual-mean flux. (b) is the latitude/season distribution of the zonal-mean flux.

model II (paper 1), using the specified mixed layer depths. The geographical distribution of the resulting annual mean heat flux into and out of the ocean surface is shown in Fig. 1a; averaged over the entire hemispheres, it yields 2.4 W m^{-2} into the Southern Hemisphere surface and an equal amount out of the Northern Hemisphere. The gross characteristics of the ocean surface heating and implied ocean heat transport appear to be realistic, with heat input at low latitudes, especially in regions of upwelling cold water, and release at high latitudes, especially in regions of poleward currents. Fig. 15 of paper 1 shows that the longitude-integrated heat transport is consistent with available knowledge of actual transports. A more comprehensive comparison with observations has been made by Miller et al. (1983), who show that the implied annual northward heat flux at the equator is 6.2×10^{14} W. With the ocean heat transport specified in this manner, the control run with computed ocean temperature has a simulated climate nearly the same as the documented model II. It is not identical, as a result of changes in the sea ice coverage which arise when the sea ice is a computed quantity. There is 15 percent less sea ice in the standard control run with computed ocean temperature than in the documented model II, as discussed below. This has local effects, mainly around Antarctica, but otherwise simulated quantities are practically identical to the documented model II climatology.

In our experiments with changed solar irradiance and atmospheric CO_2 we keep the ocean heat transport identical to that in the control run. Thus no ocean transport feedback is permitted in these experiments. Our rationale for this approach as a first step is its simplicity for analysis, and the fact that it permits a realistic atmospheric simulation.

Ocean ice cover is also computed in the experiments described here on the basis of the local heat balance. When the ocean surface loses heat, the mixed layer temperature decreases as far as the freezing point of ocean water, -1.6°C. Further heat loss from the open ocean causes ice to grow horizontally with thickness 1m until the gridbox is covered up to the limit set by the prescription for leads (open water). Still further heat loss causes the ice to thicken. Leads are crudely represented by requiring the fraction of open water in a gridbox to be greater than or equal to $0.1/z_{ice}$, where z_{ice} is the ice thickness in meters (paper 1).

Heat exchange between ocean ice and the mixed layer occurs by conduction in the climate model. A two-slab model is used for ice, with the temperature profile parabolic in each slab. This conduction is inefficient, and, if it were the only mechanism for heat exchange between the mixed layer and the ice, it would at times result in ocean ice coexisting with ocean water far above the freezing point; since this does not occur in nature, other mechanisms (such as lateral heat exchange) must contribute to the heat exchange. Therefore in our standard control run and S_o and CO_2 experiments we impose the condition that the mixed layer temperature, which represents a mean for an 8° × 10° gridbox, not be allowed to exceed 0°C until all the ice in the gridbox is melted; i.e., if the mixed layer temperature reaches 0°C additional heat input is used to meltice, decreasing its horizontal extent within the gridbox.

The annual mean sea ice cover in out standard control run is shown in Fig. 2b. Evidently there is too little sea ice in the model (15 percent less than the observations of Fig. 2a), especially at longitudes ~100°W and ~50°E in the Southern Hemisphere. Thus we also produced an alternate control run by removing the condition that all heat added to the mixed layer be used to melt ice

if the mixed layer temperature reaches 0°C. This alternate control run has about 23 percent greater ocean ice cover (Fig. 2c) than observed, and thus the standard and alternate control runs bracket observations. We use the alternate control run for a second doubled CO_2 experiment, as one means of assessing the role of ocean ice in climate sensitivity.

In the following we first describe our standard S_0 and CO_2 experiments.

S_0 and CO_2 Experiments

S_0 was increased 2 percent and CO_2 was doubled (from 315 ppm to 630 ppm) instantaneously on January 1 of year 1. Both experiments were run for 35 years. In this section we study the equilibrium response of the climate model to the S_0 and CO_2 forcings. The time dependence of the surface air temperature and the heat flux into the planetary surface are briefly noted, but only to verify that equilibrium has been achieved. The time dependence of these experiments is discussed in greater detail in a subsequent section concerned with the transient response of the climate system.

Global Mean Heat Balance and Temperature

Model II (paper 1) has a global annual mean net heat flux into the top of the atmosphere of 7.5 W m^{-2} (~2 percent of the insolation). 2.5 W m^{-2} of this imbalance is due to conversion of potential energy to kinetic energy (which is not reconverted to heat in the model) and computer truncation. The other global 5 W m^{-2} is absorbed by the ocean and ocean ice, at a rate of 7.1 W m^{-2} for the ocean surface area. This portion of the imbalance must be due to inaccuracies such as in the cloud properties, surface albedo, thermal emission calculations, etc. In our control run and experiments with computed ocean temperature we multiply the solar radiation absorbed at the ocean surface by the factor 0.96, which cancels the entire energy imbalance. The radiation correction factor has no appreciable direct effect on model sensitivity since all results are differenced against a control run; however, it does enable physical processes, such as condensation and ice melting, to operate at temperatures as realistic as possible. Together with the specified ocean transports, this allows the control run with computed ocean temperature to have essentially the same ocean temperature and climate as the model II run with fixed climatological ocean temperatures (paper 1).

The global mean heat flux into the planetary surface and surface air temperature are shown in Fig. 3 for the S_0 and CO_2 experiments. The heat flux peaks at ~3 W m^{-2} for both experiments; the radiative imbalance at the top of the atmosphere is essentially the same as this flux into the planetary surface, since the heat capacity of the atmosphere is small. Similar fluxes are expected

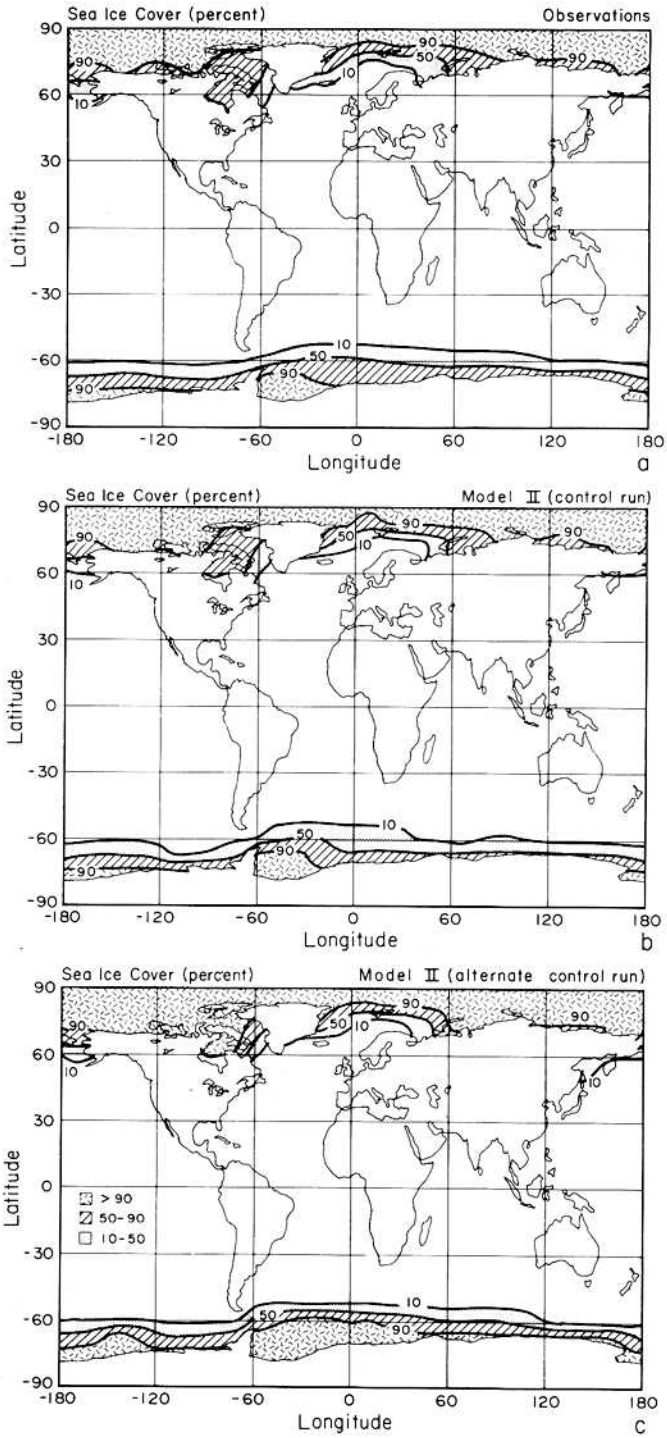

Fig. 2. Annual-mean sea ice cover. (a) observational climatology of Walsh and Johnson (1979) for the northern hemisphere and Alexander and Mobley (1976) for the southern hemisphere. (b) our standard control run of the 3-D climate model. (c) alternate control run, as described in the text.

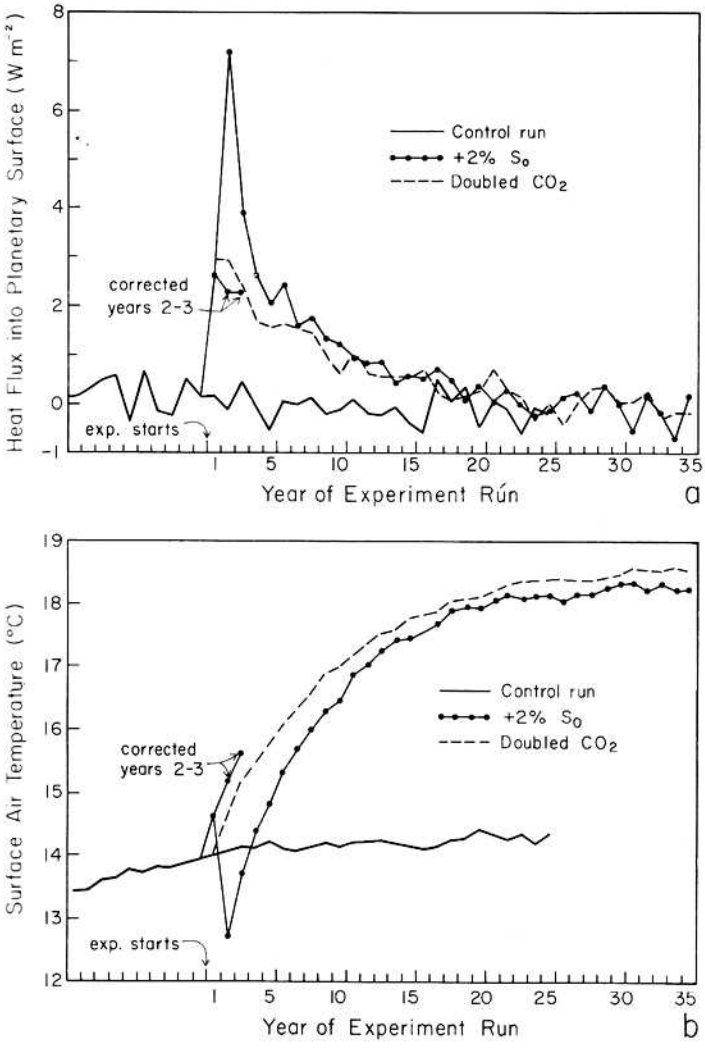

Fig. 3. Global net heat flux into planetary surface (a) and global surface air temperature (b). On April 1 of year 2 in the S_0 experiment the computer was hit by a cosmic ray or some other disturbance which caused improper numbers to be stored in the ground temperature array. This affected the temporal development of that run, but should not influence its equilibrium results. In order to determine the maximum heat flux into the ocean, the S_0 experiment was rerun for years 2 and 3 from March 31 year 2 thus eliminating the computer error for that period.

in the two experiments because of the similar magnitudes of the radiative forcings. The 2 percent S_0 change corresponds to a forcing of 4.8 W m^{-2}. The initial radiative imbalance at the top of the atmosphere due to doubling CO_2 is only ~2.5 W m^{-2}, but after CO_2 cools the stratosphere (within a few months) the global mean radiative forcing is about 4 W m^{-2} (Fig. 4, Hansen et al., 1981). Over the ocean fraction of the globe we find a peak flux into the surface of 4-5 W m^{-2} in both experiments, of order 10 percent greater than the global mean forcing for an all-ocean planet. Thus heating of the air over land with subsequent mixing by the atmosphere increases the net heat flux into the ocean, but not by the ratio of global area to ocean area as assumed by Hansen et al. (1981). Apparently heating over continental areas is balanced substantially by increased cooling to space. A chief implication is that the time constant for the ocean to respond to global heating is longer than obtained from the common practice of averaging the ocean heat capacity over the entire globe (rather than over the ocean area).

The equilibrium global mean warming of the surface air is about 4°C in both the S_0 and CO_2 experiments. This corresponds to a feedback factor f = 3-4, since the no-feedback temperature change required to restore radiative equilibrium with space is ΔT_0 = 1.2-1.3°C. The heat flux and temperature approach their new equilibria with an e-folding time of almost a decade. We show in the section on transient climate response that the e-folding time is proportional to f, and that the value inferred from Fig. 3 is consistent with f = 3-4.

The mechanisms causing the global warmings in these experiments are investigated below, including presentation of the global distribution of key changes. These results are the means for years 26-35 of the control and experiment runs. Fig. 3 indicates that this should provide essentially the equilibrium response, since by that time the heat flux into the ocean is near zero and the temperature trend has flattened out.

Global Temperature Changes

The temperature changes in the S_0 and CO_2 experiments are shown in Fig. 4 for the annual mean surface air temperature as a function of latitude and longitude, the zonal mean surface air temperature as a function of latitude and month, and the annual and zonal mean temperature as a function of altitude and latitude. We discuss the nature and causes of the temperature changes, and then make a more quantitative analysis below using 1-D calculations and the alternate CO_2 experiment with changed sea ice prescription.

The surface air warming is enhanced at high latitudes (Fig. 4, upper panel) partly due to the greater atmospheric stability there which tends to confine the warming to the lower troposphere, as shown by the radiation changes discussed below and the experiment with altered sea ice.

There is a very strong seasonal variation of the surface warming at high latitudes (Fig. 4, middle panel), due to the seasonal change of atmospheric stability and the influence of melting sea ice in the summer which limits the ocean temperature rise. At low latitudes the temperature increase is greatest in the upper troposphere (Fig. 4, lower panel), because the added heating at the surface primarily causes increased evaporation and moist convection, with deposition of

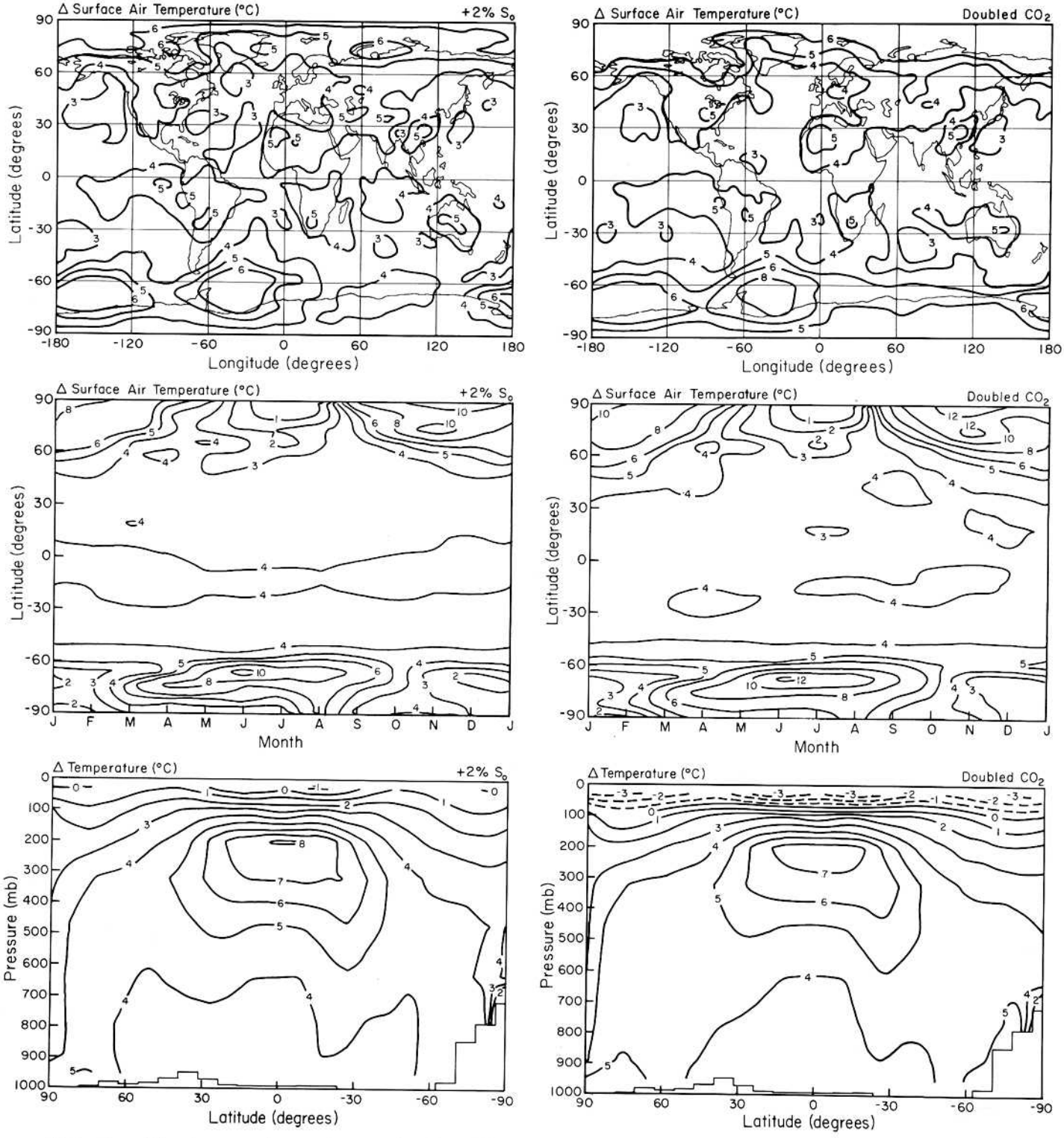

Fig. 4. Air temperature change in the climate model for a two percent increase of solar irradiance (left) and for doubled atmospheric CO_2 (right). The upper graphs show the geographical distribution of annual mean surface air warming, the middle graphs show the seasonal variation of the surface air warming averaged over longitude, and the lower graphs show the altitude distribution of the temperature change averaged over season and longitude.

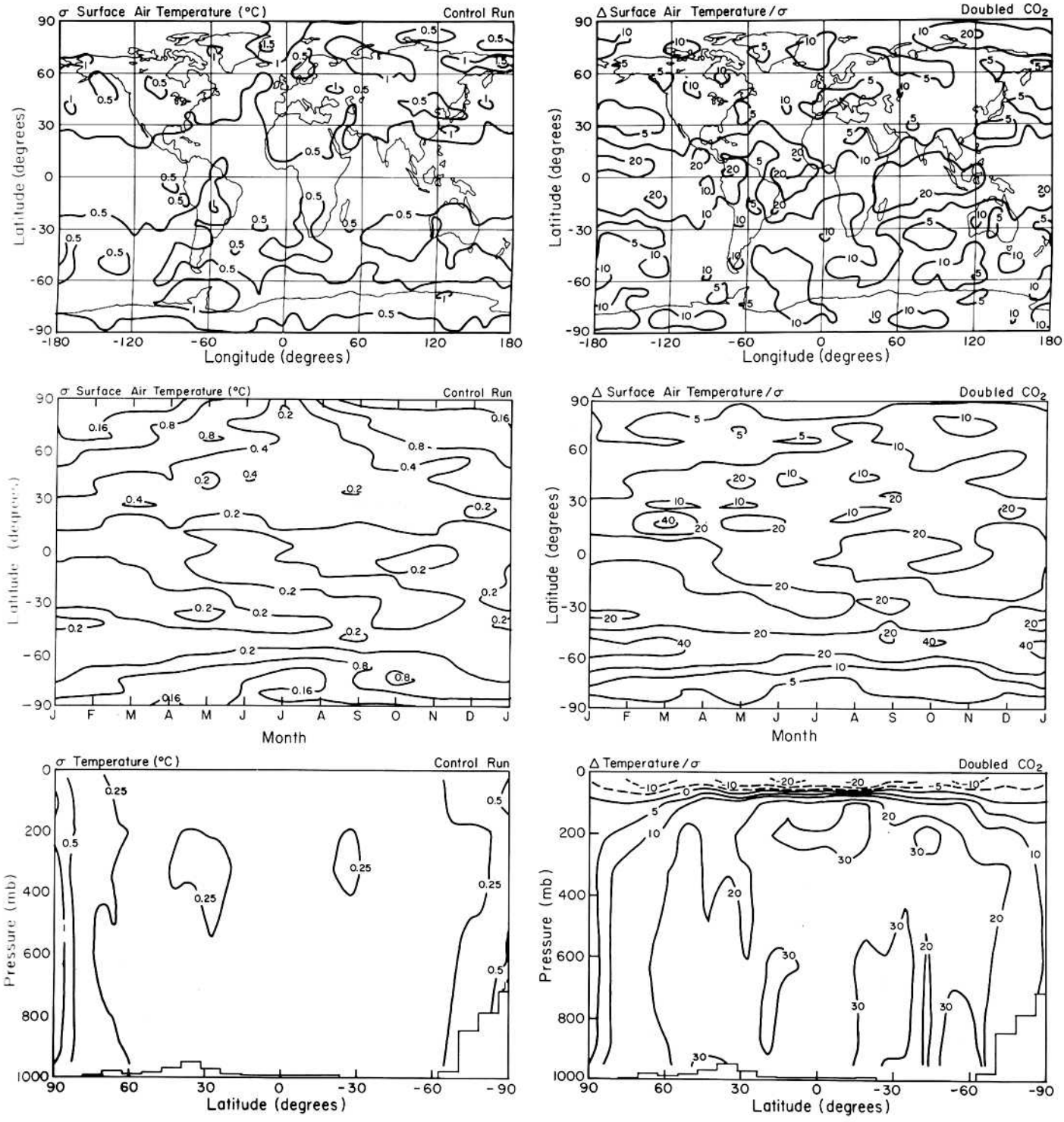

Fig. 5. Left side: standard deviation of temperature for the last 10 years in the control run. Right side: ratio of temperature change for years 26-35 of the doubled CO_2 experiment to the standard deviation of temperature in the control run.

latent heat and water vapor at high levels.

The statistical significance of these results can be verified from Fig. 5, which shows the standard deviation for the last 10 years of the control run for all the quantities in Fig. 4, and the ratio of the change of the quantity in the doubled CO_2 experiment to the standard deviation. The standard deviation is computed routinely for all of the quantities output from our 3-D model. We only discuss changes in the experiment runs

which are far above the level of model fluctuations or 'noise' in the control run.

The patterns of temperature change are remarkably similar in the S_0 and CO_2 experiments, suggesting that the climate response is to first order a function of the magnitude of the radiative forcing. The only major difference is in the temperature change as a function of altitude; increased CO_2 causes substantial stratospheric cooling. This similarity suggests that, to first order, the climate effect due to several forcings including various tropospheric trace gases may be a simple function of the total forcing.

The global mean warming of surface air that we obtain for doubled CO_2 is similar to that obtained by Manabe and Stouffer (1980) for quadrupled CO_2. This large difference in sensitivity of the two models appears to be associated mainly with the feedback mechanisms in the models, as discussed below. The patterns of the temperature changes in the two models show gross similarities, but also significant differences. We defer detailed comparison of the model results until after discussion of the feedback mechanisms.

1-D Analysis of Feedbacks in 3-D Experiments

The processes chiefly responsible for the temperature rise in the 3-D model can be investigated with a 1-D radiative convective (RC) climate model. We use the 1-D model of Lacis et al. (1981) to evaluate the effect of changes in radiative forcing that take place in the 3-D model experiments. As part of the 3-D model diagnostics, we have available global average changes in surface and planetary albedo, and changes in amount and vertical distribution of clouds, water vapor and atmospheric lapse rate. We insert these changes one-by-one, or in combination, into the 1-D model and compute the change in global surface temperature. We employ the usual 'convective adjustment' procedure in our 1-D calculations, but with the global mean temperature profile of the 3-D model as the critical lapse rate in the troposphere. Contrary to usual practice, we allow no feedbacks to operate in the 1-D calculations, making it possible to associate surface temperature changes with individual feedback processes.

There is no a priori guarantee that the net effect of these changes will yield the same warming in the 1-D model as in the 3-D model, because simple global and annual averages of the changes do not account for the nonlinear nature of the physical processes and their 2-D and 3-D interactions. Also, changes in horizontal dynamical transports of heat and moisture are not entered explicitly into the 1-D model; the effects of dynamical feedbacks are included in the radiative factors which they influence, such as the cloud cover and moisture profile, but the dynamical contributions are not identified. Nevertheless, this exercise provides substantial information on climate feedbacks. Determination of how well the 1-D and 3-D results correspond also is a useful test for establishing the value of 1-D global climate models.

The procedure we use to quantify the feedbacks is as follows. The increase of total water vapor in the 3-D model (33 percent in the S_0 experiment) is put in the 1-D model by multiplying the water vapor amount at all levels by the same factor (1.33); the resulting change in the equilibrium surface temperature of the 1-D model defines the second bars in Fig. 6. Next the water vapor at each level in the 1-D model is increased by the amount found in the 3-D experiment; the temperature change obtained in the first (total H_2O amount) test is subtracted from the temperature change obtained in this test to obtain the temperature change credited to the change in water vapor vertical distribution. The change of temperature gradient (lapse rate) between each pair of levels in the 3-D model is inserted in the control 1-D model to estimate the effect of lapse rate change on surface temperature, shown by the fourth bars in Fig. 6. Since the lapse rate changes are due mainly to changes of water vapor, we take the net of these three temperature changes in the 1-D model as our estimate of the water vapor contribution to the total temperature change. The global mean ground albedo change in the 3-D model (defined as the ratio of the global mean upward and downward solar radiation fluxes at the ground) is inserted into the 1-D control run to obtain our estimate of the ice/snow albedo contribution to the temperature change.

Cloud contributions are more difficult to analyze accurately because of the variety of cloud changes that occur in the 3-D model (see below), including changes in cloud overlap, and the fact that the changes do not combine linearly. We first estimate the total cloud impact by changing the cloud amounts at all levels in the 1-D model in proportion to changes obtained in the 3-D model. The total cloud effect on the temperature obtained in this way is subdivided by defining a portion to be due to the cloud cover change (by running the 1-D model with a uniform change of all clouds so as to match the total cloud cover change in the 3-D model) and by assigning the remainder of the total cloud effect to cloud height changes. These assumptions involve some arbitrariness. Nevertheless, the resulting total temperature changes in the 1-D model are found to be within 0.2°C of the global mean temperature changes in the 3-D experiments, providing circumstantial evidence that the procedure takes into account the essential radiative aspects of cloud cover change.

The temperature changes in the 1-D model are shown in Fig. 6 for the standard S_0 and CO_2 experiments, and the CO_2 experiment with alternate sea ice computation. Resulting gains and feedback factors are given in Table 1.

Water vapor feedback. Water vapor provides

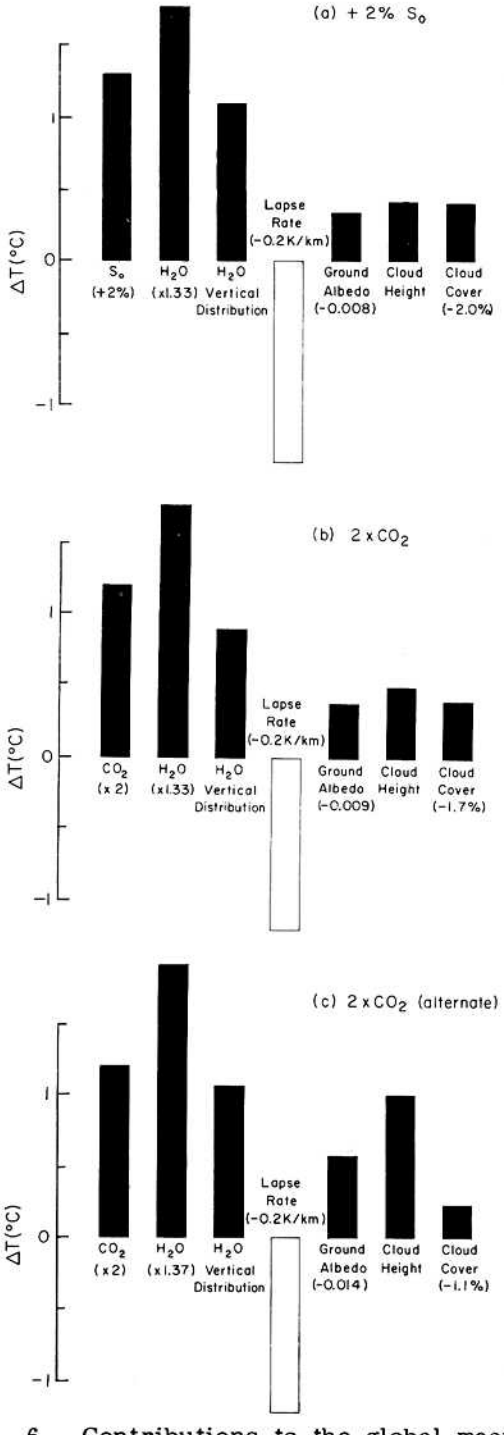

Fig. 6. Contributions to the global mean temperature rise in the S_0 and CO_2 experiments as estimated by inserting changes obtained in the 3-D experiments into 1-D radiative convective model. (a) +2 percent S_0 experiment, (b) doubled CO_2 experiment, and (c) doubled CO_2 experiment for alternate control run with greater sea ice.

the largest feedback, with most of it caused by the increase of water vapor amount. Additional positive feedback results from the water vapor distribution becoming weighted more to higher altitudes, but for the global and hemispheric means this is approximately cancelled by the negative feedback produced by the changes in lapse rate, also due mainly to the added H_2O. The near cancellation of these two effects is not surprising, since the amount of water the atmosphere holds is largely dependent on the mean temperature, and the temperature at which the infrared opacity occurs determines the infrared radiation. This tendency for cancellation suggests that the difficulty in modeling moist convection and the vertical distribution of water vapor may not have a great impact on estimates of global climate sensitivity (excluding the indirect effect on cloud distributions).

The net water vapor gain thus deduced from the 3-D model is $g_w \sim 0.4$, or a feedback factor $f_w \sim 1.6$. The same sensitivity for water vapor is obtained in 1-D models by using fixed relative humidity and fixed critical lapse rate (Manabe and Wetherald, 1967), thus providing some support for that set of assumptions in simple climate models. Relative humidity changed only slightly in our 3-D experiments; for example, in our standard doubled CO_2 experiment the average relative humidity increased 0.015 (1 = 100 percent humidity), with a 0.06 global increase at 200 mb being the largest change at any altitude. This compares with an increase of mean specific humidity of 33 percent. The global mean lapse rate change in the 3-D model ($-0.2°C\ km^{-1}$) is less than the change of the moist adiabatic lapse rate ($-0.5°C\ km^{-1}$), the decrease at low latitudes being partly offset by an increase at high latitudes. And, as explained above, the effect of the lapse rate change on temperature is largely balanced by the effect of the resulting displacement of water vapor to greater altitude.

Snow/ice feedback. Ground albedo decrease also provides a positive feedback. The ground albedo change (upper panel of Fig. 7) is largely due to reduced sea ice. Shielding of the ground by clouds and the atmosphere (middle panel of Fig. 7) makes this feedback several times smaller than it would be in the absence of the atmosphere. However, it is a significant positive feedback and is at least as large in the Southern Hemisphere as in the Northern Hemisphere. The geographic pattern of the temperature increase (Fig. 4) and the coincidence of warming maxima with reduced sea ice confirm that the sea ice effect is a substantial positive feedback.

Further insight into the sea ice feedback is provided by the experiment with alternate prescription for computing sea ice cover. The greater sea ice cover in the control run for this experiment permits a greater surface albedo feedback, as indicated by the analysis with the 1-D model shown in Fig. 6c. These results illustrate the sensitivity of a system which already contains large positive feedbacks, the gain due to increased surface albedo being augmented by in- water vapor and cloud gains.

Based on these experiments, we estimate the sea ice/snow feedback factor as ~1.1. However,

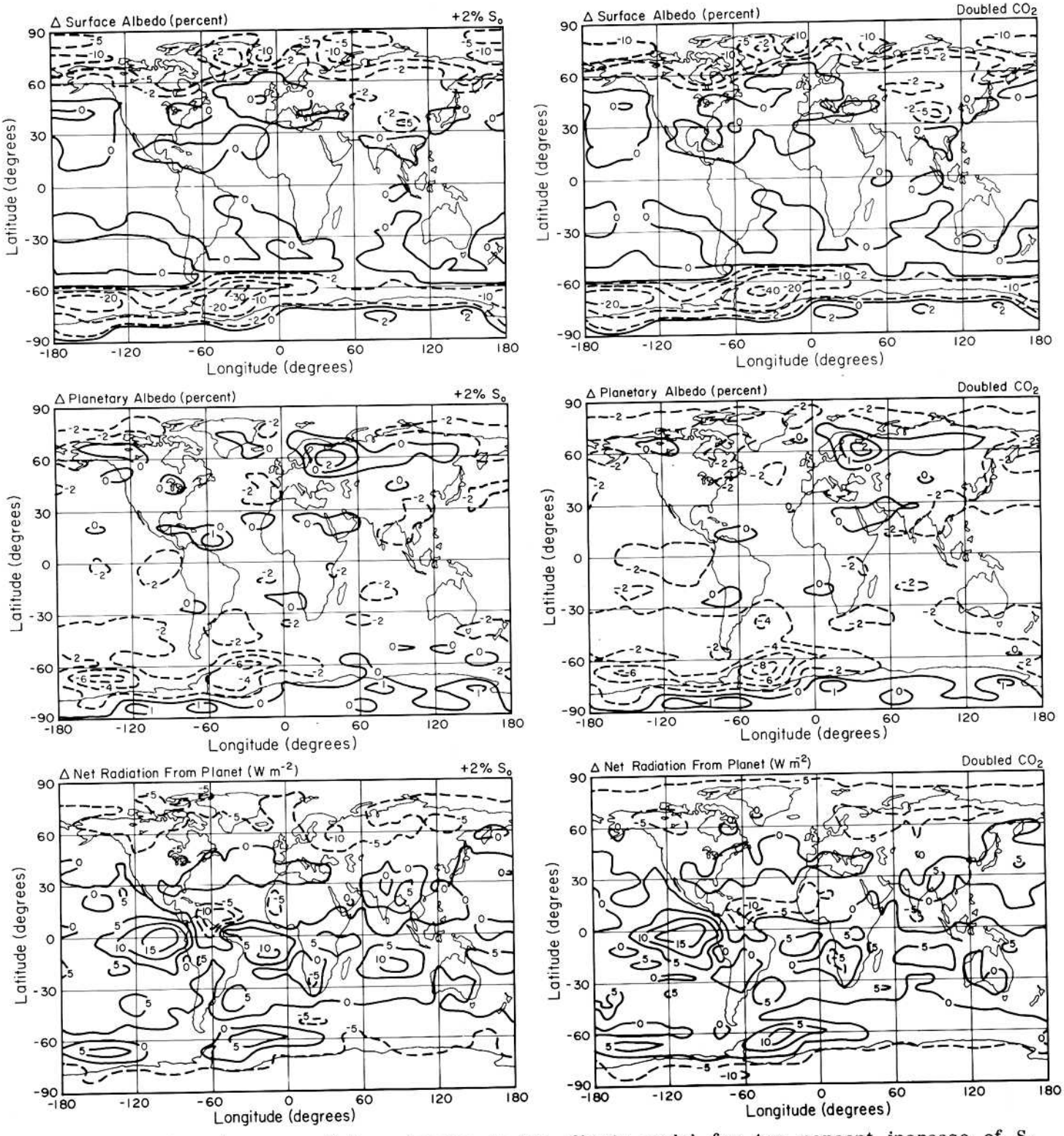

Fig. 7. Annual mean radiation changes in the climate model for two percent increase of S_0 (left) and doubled CO_2 (right). In Figs. 7, 8, 10 and 11 "percent" change refers to the full range of the quantity, e.g., a change from 60 percent albedo to 50 percent albedo is defined to be a 10 percent change.

this value refers to a climate change from today's climate to a climate which is warmer by about 4°C. We expect $f_{snow/ice}$ to decrease as the area of sea ice and snow decreases, so its value is probably somewhat larger in the limit of a small increment about today's climate. Also, the prescription for computing sea ice in our standard experiments (which gives 15 percent too little sea ice for today's climate) probably causes an underestimate of $f_{snow/ice}$, as indicated by the value inferred for f in the experiment with al tered sea ice prescription (which yielded 23 percent too much sea ice for today's climate).

The gain we obtain for ice/snow feedback in our 3-D model (~0.1) agrees well with the value (0.12) obtained by Wang and Stone (1980) from a 1-D radiative convective model. The feedback is much smaller than early estimates such as those of Budyko (1969) and Sellers (1969), who assigned a large albedo increment to ice/snow, but did not account for cloud shielding, vegetation masking of snow, and zenith angle variation of albedo (North, 1975; Lian and Cess, 1977).

Cloud feedback. Cloud changes (Fig. 8) also provide a significant positive feedback in this model, as a result of a small increase in mean cloud height and a small decrease in cloud cover. The gain we obtain for clouds is 0.22 in our standard doubled CO_2 experiment. This happens to be similar to the gain of 0.19 which is obtained in 1-D models if the cloud cover is kept fixed and the cloud height is determined by the assumption of fixed cloud temperature (Cess, 1974). However, a substantial part of the cloud gain in the 3-D model is due to the cloud cover change (Fig. 6). The portion of the cloud gain associated with cloud height change in the S_0 experiment and the standard doubled CO_2 experiment is about midway between the two common assumptions used in simple climate models: fixed clouds altitude (gain = 0) and fixed cloud temperature (gain = 0.2).

The cloud height and cloud cover changes in the 3-D model seem qualitatively plausible. The reduced cloud cover primarily represents reduction of low and middle level clouds, due to increased vertical transport of moisture by convection and the large scale dynamics. The increase of high level cirrus clouds at low latitudes is consistent with the increase of penetrating moist convection at those latitudes. However, the cloud prescription scheme in the model (paper 1) is highly simplified; for example, it does not incorporate a liquid water budget for the cloud droplets or predict changes in cloud optical thickness at a given height. Thus the possibility of an increase in mean cloud optical thickness with the increased water vapor content of the atmosphere is excluded. Indeed, because the cloud optical thickness decreases with increasing altitude (paper 1), the increase of cloud height causes a decrease of optical thickness. This is a positive feedback for low and middle level clouds, but a negative feedback for cirrus clouds, which are a greenhouse material with suboptimal optical thickness. As a crude test of possible effects of changes in cloud optical thickness we let the cloud optical thickness in the 1-D model change in proportion to the absolute humidity: this practically eliminated the positive cloud feedback, i.e., it resulted in $f_{clouds} \sim 1.0$. Clearly, assessment of the cloud contribution to climate sensitivity depends crucially upon development of more realistic representation of cloud formation processes in climate models, as verified by an accurate global cloud climatology.

Summary of model feedbacks. Given the cancellation between the change in lapse rate and change in vertical distribution of water vapor, the processes providing the major radiative feedbacks in this climate model are total atmospheric water vapor, clouds and the surface albedo. Considering the earth from a planetary perspective, it seems likely that these are the principal feedbacks for the earth on a time scale of decades. The albedo of the planet for solar radiation is primarily determined by the clouds and surface, with the main variable component of the latter being the ice/snow cover. The thermal emission of the planet is primarily determined by the atmospheric water vapor and clouds. Thus the processes principally responsible for the earth's radiation balance and temperature are included in the 1-D model, and we have shown that these processes are the source of the primary radiative feedbacks in our 3-D model.

Table 1 summarizes the gains and feedback factors inferred from the changes which occurred in our 3-D model experiments, and the corresponding temperature changes for different combinations of these feedback processes. Note again that effects of dynamical feedbacks are implicitly included in these changes. The temperature changes illustrate the nonlinear way in which feedback processes combine [Eq. (9)]. For example, the ice/snow feedback adds about 1°C to the temperature response, but if the water vapor and cloud feedbacks did not exist the ice/snow feedback would add only a few tenths of a degree to the sensitivity. This nonlinear behavior is a result of the fact that when the ice/snow feedback occurs in the presence of the other (positive) feedbacks, it enhances the water vapor and cloud changes.

Comparison to Manabe and Stouffer. This analysis of the feedbacks in our model provides an indication of the causes of the difference between our climate model sensitivity and that of Manabe and Stouffer (1980). They infer a warming of 2°C for doubled CO_2, based on an experiment with quadrupled CO_2 which yielded 4°C warming. Their model had fixed clouds (altitude and cloud cover), thus $f_{cloud} \equiv 1$. Also their control run had less sea ice than our model, so their $f_{sea\ ice}$ should be between 1 and the value (~1.1) for our model. It is apparent from Table 1 that differences arising from the treatments of these two processes may account for most of the difference in global climate sensitivity.

Another major difference between our model

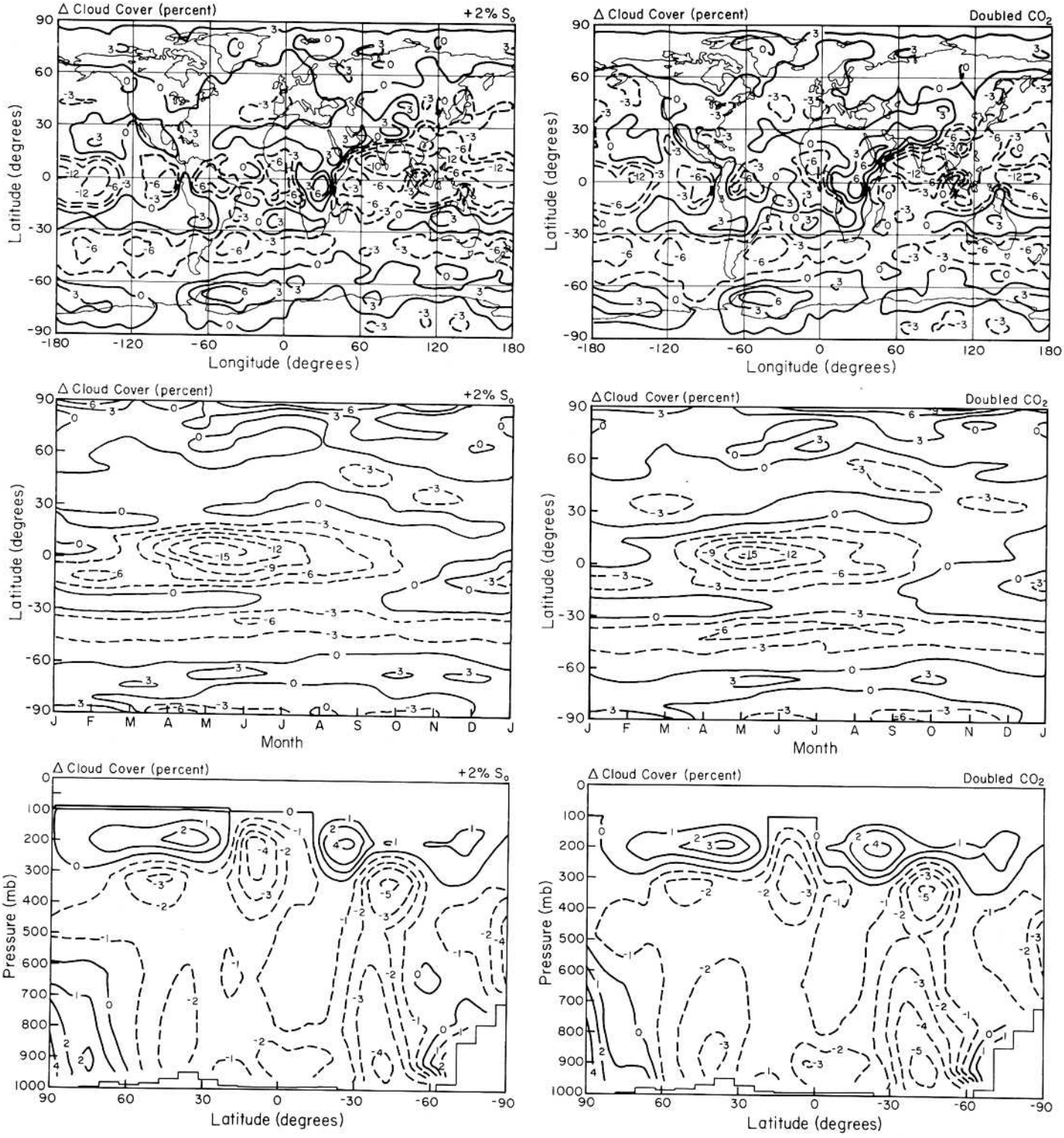

Fig. 8. Cloud changes in the climate model for two percent increase of S_0 (left) and doubled CO_2 (right). The upper graphs show the geographical distribution of annual mean cloud cover change, the middle graphs show the seasonal variation of cloud cover change averaged over longitude, and the lower graphs show the altitude distribution of the cloud cover change averaged over season and longitude.

TABLE 1. Gain (g), feedback factor (f) and equilibrium temperature changes (ΔT) inferred from calculations with 1-D radiative-convective model for global mean changes in the 3-D GCM experiments. The subscripts w, c and s refer to water vapor, clouds and surface albedo. g is obtained as the ratio of the temperature change in the 1-D model (with only the indicated processes included) to the global mean temperature change in the 3-D experiment. f is from $f_i = 1/(1 - g_i)$. ΔT is the equilibrium surface air warming computed with the 1-D model for global mean changes of 3-D model constituents with only the indicated processes included; ΔT_o includes only the indicated radiative forcing, without feedbacks.

	Experiment		
	+2% S_o	Doubled CO_2	Alternate Doubled CO_2
g_w	0.37	0.40	0.37
g_c	0.20	0.22	0.26
g_s	0.09	0.09	0.12
f_w	1.59	1.66	1.58
f_c	1.26	1.29	1.34
f_s	1.09	1.10	1.14
f_{wc}	2.36	2.62	2.67
f_{wcs}	2.96	3.45	3.95
ΔT_o	1.3	1.2	1.2
ΔT_{ow}	2.1	2.0	1.9
ΔT_{oc}	1.7	1.6	1.6
ΔT_{os}	1.5	1.3	1.4
ΔT_{owc}	3.2	3.2	3.2
ΔT_{owcs}	4.0	4.2	4.8

and the model of Manabe and Stouffer is that we include a specified horizontal transport of heat by the ocean. This transport is identical in our control and experiment runs, i.e., the changed climate is not allowed to feed back on the ocean circulation. Of course Manabe and Stouffer do not allow feedback on ocean transport either, since the ocean transport is zero in both experiment and control. However, some other mechanisms must replace oceanic poleward transport of heat in their model, since their high latitude temperatures are at least as warm as in our model (and observations). Enhanced poleward transport of latent and sensible heat by the atmosphere must be the mechanism replacing ocean heat transport in their model. This atmospheric transport is expected to provide a negative feedback (Stone, 1984), and indeed the total atmospheric energy transport did decrease poleward of 50°C latitude in the CO_2 experiments of Manabe and Wetherald (1975, 1980). It is not obvious whether the ocean transport feedback is positive or negative in the real world.

The contribution of ocean heat transport to climate sensitivity, like that of the atmospheric transports, does not appear as an identified component in an energy balance analysis such as in Fig. 6. This is irrelevant for our model, since it has no ocean transport feedback. However, in models which calculate the ocean heat transport or a surrogate energy transport, this feedback is included implicitly as a (positive or negative) portion of identified components of ΔT ($\Delta T_{water\ vapor}$, ΔT_{clouds}, $\Delta T_{ice/snow}$). The portion of these changes due to this feedback process could be identified by running those models with fixed (climatological) ocean heat transport.

Manabe (1983) suggests that our ice/snow feedback is unrealistically large and accounts for most of the difference between our climate model sensitivity and that of Manabe and Stouffer (1980). However, as summarized in Table 2, the amount of sea ice in the control run for our standard CO_2 experiment is actually somewhat less than observed sea ice cover. In our alternate CO_2 experiment, with sea ice cover greater than in observations, the ice/snow feedback increases significantly, suggesting that the ice/snow feedback in our standard experiment may be an underestimate. Also, we show in the next section that the sea ice feedback for the climate change from 18K to today, a warming of about 4°C, is about twice as large as in our doubled CO_2 experiments; this 18K sea ice feedback factor is based on measured changes of sea ice cover. The small ice/snow feedback in Manabe and Stouffer's model may be a result of their model being too warm at high latitudes; indeed, in the Southern Hemisphere (where the sea ice feedback is greatest in our model and in 18K measurements) their control run has almost no ice in the summer. Another likely reason for Manabe and Stouffer's albedo feedback being weaker is the stronger negative feedback in their meridional dynamical flux, as a result of that flux all being carried in the atmosphere. We conclude that our estimate for the sea ice feedback is conservative, i.e., it is more likely to be in error on the low side than on the high side.

We obtain a greater warming at low latitudes (~3-4°C for doubled CO_2) than that found by Manabe and Stouffer (~3°C for quadrupled CO_2). We analyzed the contributions to the warming in our 3-D model as a function of latitude by inserting all zonal-mean radiative changes into the 1-D radiative-convective model. At low latitudes (0-30°) the clouds contribute a positive feedback of about 1-1.5°C; the larger part of this, nearly 1°C, is due to reduction of low level cloud cover with doubled CO_2, with increase of cirrus clouds contributing a smaller positive feedback. At high latitudes (60-90°) the clouds contribute a smaller negative feedback (0-1°C), due to increased low level clouds; this cloud increase (Fig. 8) probably is due to increased evaporation resulting from the reduced sea ice cover. The computed distributions of water vapor may also contribute

TABLE 2. Annual-mean sea ice cover as fraction of global or hemispheric area in several 3-D experiments. In run 1 the sea ice cover is specified to be today's climatology of Alexander and Mobley (1976) for the Southern Hemisphere and Walsh and Johnson (1979) for the Northern Hemisphere. Run 7 specifies the sea ice cover according to CLIMAP data for 18K (CLIMAP, 1981) and run 11 modifies the Southern Hemisphere CLIMAP data as discussed in the section on ice age experiments. In other runs the sea ice cover is computed.

Run	Experiment Description	Sea Ice Cover		
		Globe	Northern Hemisphere	Southern Hemisphere
1	Model II, Run 61 of paper 1; sea ice specified as today's climatology	0.048	0.042	0.054
2	Control run for standard CO_2 and S_0 experiments	0.041	0.039	0.043
3	Standard 2 × CO_2 experiment	0.023	0.028	0.017
4	Standard +2% S_0 experiment	0.025	0.030	0.020
5	Control run for alternate CO_2 experiment	0.060	0.046	0.073
6	Alternate 2 × CO_2 experiment	0.031	0.033	0.029
7	CLIMAP boundary conditions	0.089	0.048	0.131
11	CLIMAP boundary conditions with modified Southern Hemisphere sea ice	0.077	0.048	0.106

to the difference between our result and that of Manabe and Stouffer. For example, in our model low latitude relative humidity at 200 mb increased by 0.085 with doubled CO_2. The cloud and water vapor characteristics depend on the modeling of moist convection and cloud formation; Manabe and Stouffer use the moist adiabatic adjustment of Manabe et al. (1965) and fixed clouds; we use a moist convection formulation which allows more penetrative convection (paper 1) and cloud formation dependent on local saturation. Presently available cloud climatology data has not permitted detailed evaluation of these moist convection and cloud formation schemes.

The high latitude enhancement of the warming is less in our model than in observed temperature trends for the past 100 years (Hansen et al., 1983a). If this observed high latitude enhancement also occurs for large global temperature increases, the smaller high latitude enhancement in our 3-D model suggests the possibility that the 3-D model has either overestimated the low latitude climate sensitivity (probably implicating the low latitude cloud feedback) or underestimated the high latitude sensitivity. If the former case is correct, the global climate sensitivity implied by the 3-D model may be only 2.5-3°C; but if the latter interpretation is correct, the global climate sensitivity may be greater than 4°C. A more precise statement requires the ability to analyze and verify the cloud feedback on a regional basis.

Conclusion. Atmospheric water vapor content provides a large positive feedback, and we find that in our model the effects of changes in lapse rate and water vapor vertical distribution largely cancel (for global or hemispheric means). The existence of the strong positive water vapor feedback implies that moderate additional positive feedback can greatly increase climate sensitivity, because of the nonlinear way in which feedbacks combine. In our model, sufficient ice/snow feedback occurs to increase the global sensitivity to ~2.5°C, and with cloud feedback to ~4°C for doubled CO_2. Although the cloud feedback is very uncertain, our 3-D study suggests that it is in the range from approximately neutral to strongly positive in global mean, and thus that global climate sensitivity is at least 2.5°C for doubled CO_2. The magnitudes of the global ice/snow and cloud feedbacks in our 3-D model are plausible, but confirmation requires improved ability to accurately model the physical processes as well as empirical tests of the climate model on a variety of time scales.

Ice Age Experiments

Records of past climate provide a valuable means to test our understanding of climate feedback mechanisms, even in the absence of a complete understanding of what caused the climate change. In this section we use the comprehensive reconstruction of the last ice age (18,000 years ago) compiled by the CLIMAP project (CLIMAP project members, McIntyre, project leader, 1981; Denton and Hughes, 1981). We first run our climate model with the 18K boundary conditions as specified by CLIMAP; this allows us to estimate the global mean temperature change between 18K and today. We then rerun the model changing feedback processes one-by-one and note their effect on the planetary radiation balance at the top of the atmosphere. This provides a measure of the gain or feedback factor for each process. We also examine the model for radiation balance when all of the known 18K feedbacks are included; this allows some inferences about the model sensitivity and the accuracy of the CLIMAP data. Finally, we compare different contributions to the 18K cooling; by considering the land ice and atmospheric CO_2 changes as slow or specified global climate forcings, we can infer empirically the net feedback factor for processes operative on 10-100 year time scales.

Global maps of the CLIMAP 18K boundary conditions, including the distributions of continental ice, sea ice and sea-surface temperature, are given by CLIMAP (1981) and Denton and Hughes (1981). These boundary conditions, obtained from evidence such as glacial scouring, ocean sediment cores containing detritus rafted by sea ice, and oxygen isotopic abundances in snowfall preserved in Greenland and Antarctic ice sheets, necessarily contain uncertainties. For example, Burckle et al. (1982) suggest that the CLIMAP Southern Hemisphere sea ice cover may be overestimated, and DiLabio and Klassen (1983) argue that the CLIMAP 'maximum extent' ice sheet model may be an overestimate. Questions have also been raised about the accuracy of the ocean surface temperatures, especially at low latitudes (Webster and Streten, 1978). We examine quantitatively the effect of each of these uncertainties on our feedback analyses.

Simulated 18K Climate Patterns

Our 18K simulation was obtained by running climate model II (paper 1) with the CLIMAP (1981) boundary conditions. The boundary conditions included the earth orbital parameters for that time (Berger, 1978). The run was extended for six years, with the results averaged over the last five years to define the 18K simulated climate. The control run was the five year run of model II with today's boundary conditions, which is documented in paper 1.

Temperature. Simulated 18K temperature patterns are shown in Fig. 9. The temperatures in the model, especially of surface air, are constrained strongly by the fixed boundary conditions, and thus their accuracy is dependent mainly on the reliability of the CLIMAP data.

Global surface air temperature in the 18K experiment is 3.6°C cooler than in the control run for today's boundary conditions. Much greater cooling, exceeding 20°C, occurs in southern Canada and northern Europe and cooling of more than 5°C is calculated for most of the Southern Hemisphere sea ice region. Some high latitude regions, including Alaska and parts of Antarctica, are at about the same temperature in the 18K simulation as today; thus there is not universal high latitude enhancement of the climate change.

Temperature changes over the tropical and subtropical oceans are only of the order of 1°C, and include substantial areas that are warmer in the 18K simulation than today. The latter aspect requires verification; diverse areas of the tropics and subtropics experienced mountain glaciation at 18K with snowline descent of about 1km, and pollen data indicate substantial cooling of the order of 5°C at numerous low latitude areas. As indicated by our 3-D model experiment the CLIMAP sea surface temperatures are inconsistent with the observations of tropical cooling, since specification of relatively warm tropical and subtropical ocean temperatures effectively prohibits large cooling over land at these latitudes. We conclude that the low latitude ocean temperatures are probably overestimated in the CLIMAP data. A more quantitative analysis (Rind and Peteet, in preparation) suggests that large areas in the low latitude oceans may be too warm by 2-3°C in the CLIMAP data.

The middle parts of Fig. 9 show that the cooling at 18K occurred especially in the fall and winter. Although the surface air was substantially colder all year at latitude 60°N, this was largely a result of the change in mean surface altitude caused by the presence of ice sheets; the cooling at fixed altitude is considerably less. The zonal mean surface air in the tropics was cooler all year. The lower parts of Fig. 9 show substantial cooling throughout most of the troposphere. At high latitudes the greatest cooling occurs in the lower troposphere.

Radiation. Changes in the planetary radiation budget in the 18K simulation are shown in Fig. 10. The surface albedo increases as much as 0.45 in the regions of ice sheets over northern Europe and southern Canada and about 0.30 in regions of large changes in sea ice coverage. Shielding by the atmosphere and the large zenith angles reduce the impact on planetary albedo to 0.15-0.20 over the ice sheets and 0.05-0.10 over sea ice. The effect of the planetary albedo change on the net radiation from the planet is partially compensated over the ice sheets by reduced thermal emission, but nearly the full effect of the albedo change appears in the net radiation change over sea ice; these conclusions follow from comparison of the middle and lower parts of Fig. 10 and the fact

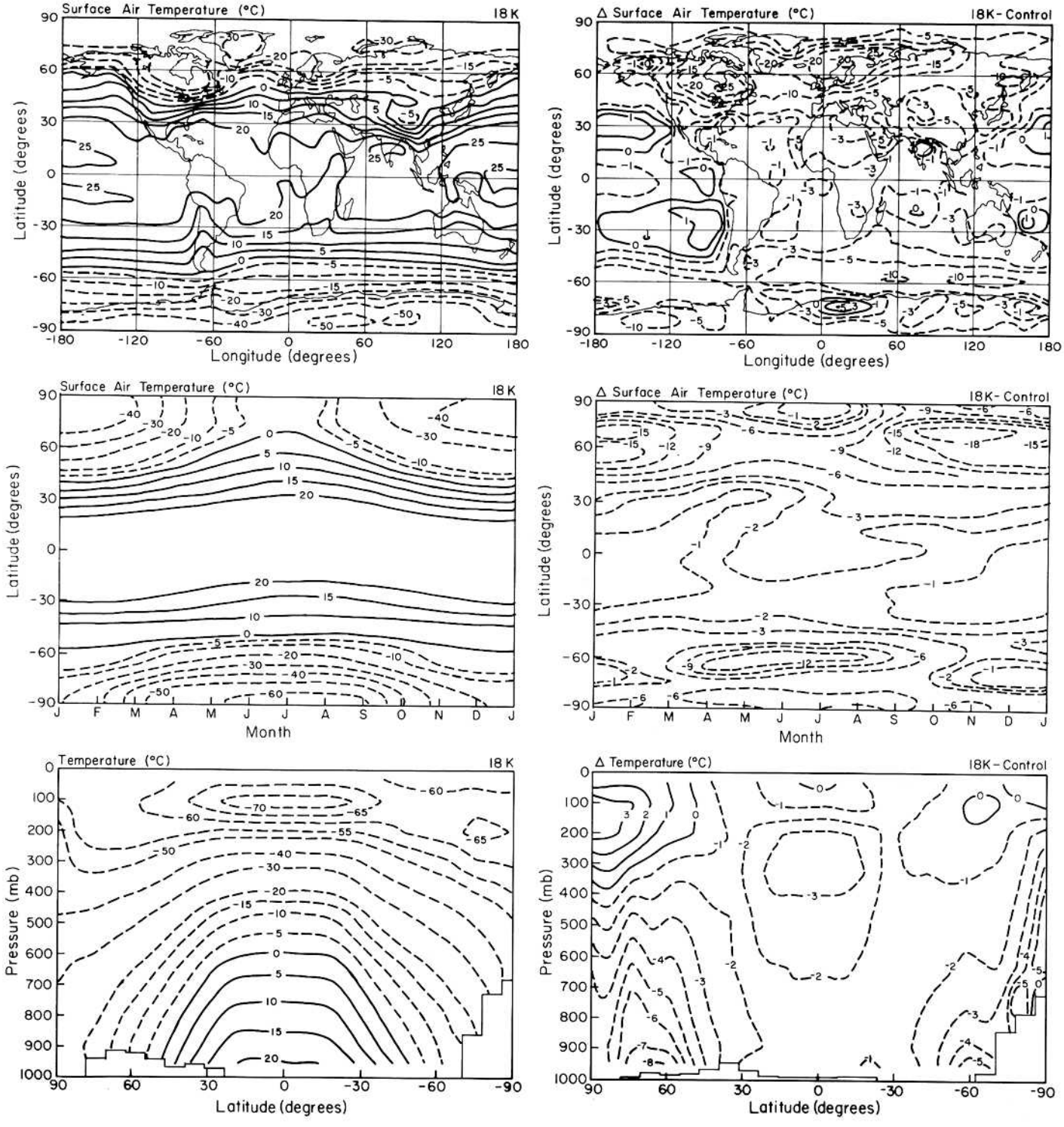

Fig. 9. Air temperature in the climate model experiment with boundary conditions for the ice age 18,000 years ago (left) and the temperature difference between the 18K simulation and the control run for today's climate boundary conditions (right). The control run is described in detail in paper 1.

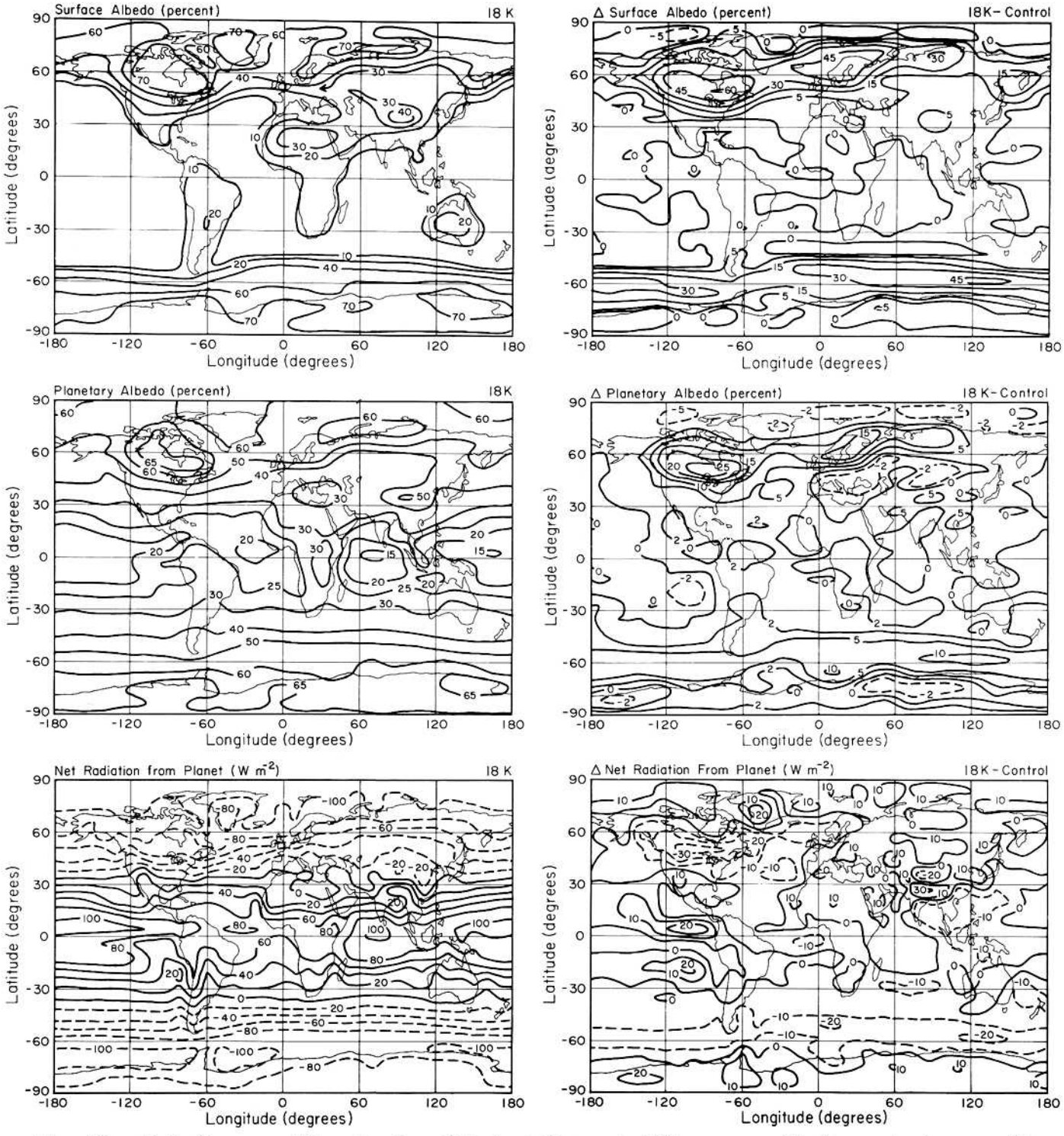

Fig. 10. Radiation quantities for the 18K simulation and differences with the control run. The control run is described in detail in paper 1.

that an albedo change of 0.10 is equivalent to 24 W m^{-2}. Most of the more detailed changes in the geographical patterns of the radiation budget are associated with changes of cloud cover or cloud top altitude.

Clouds. Cloud changes in the 18K simulation are illustrated in Fig. 11. There is a significant reduction of cloud cover in regions with increased sea ice, probably because of the reduced evaporation in those regions. The zonal

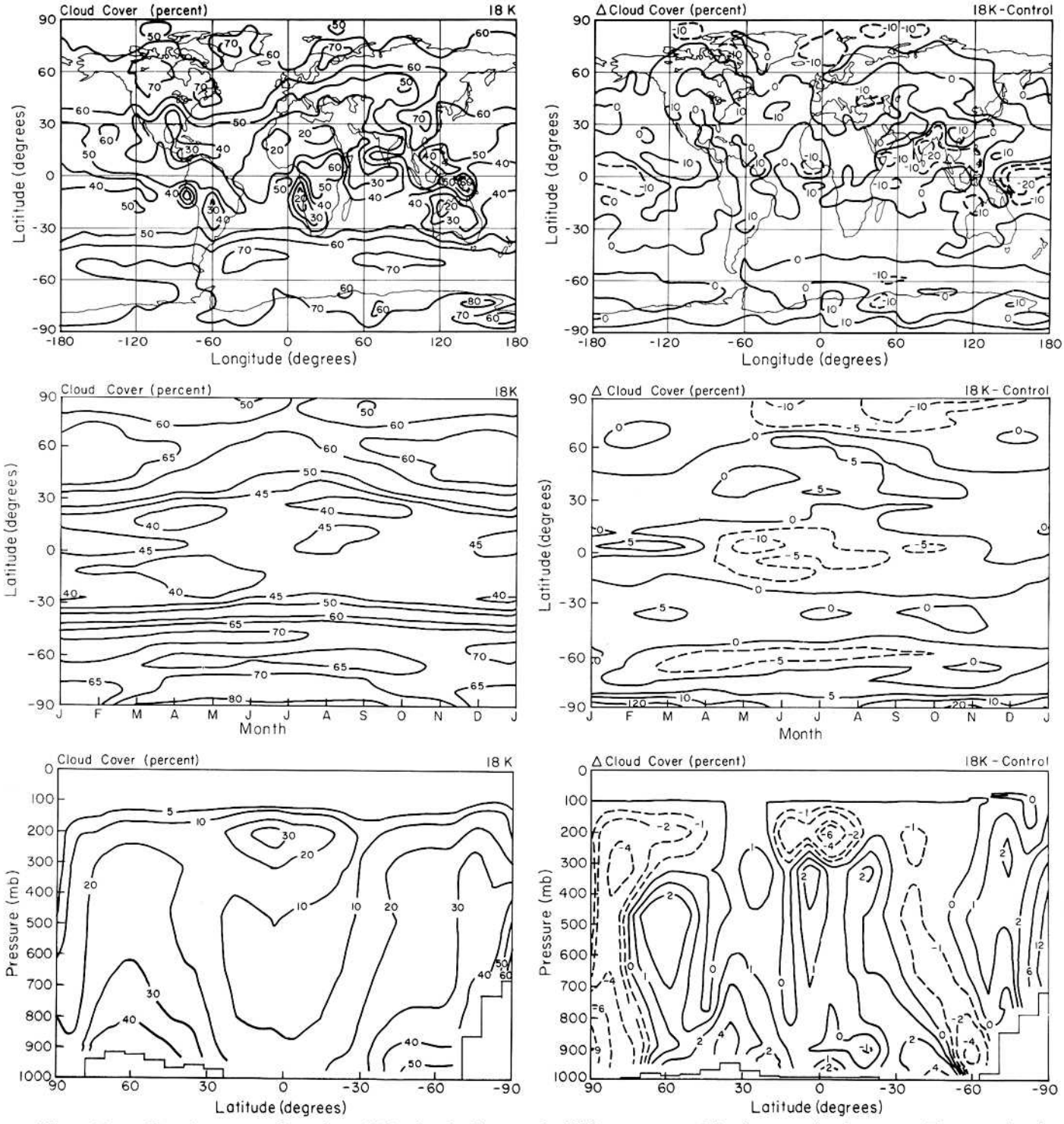

Fig. 11. Cloud cover for the 18K simulation and differences with the control run. The control run is described in detail in paper 1.

mean cloud cover decreases slightly in the tropics during most of the year, increases slightly in the subtropics and increases at Northern Hemisphere midlatitudes in summer. The polar regions exhibit opposite behavior; at the north pole (a region of sea ice) the clouds decrease, while at the south pole (a continental region of high topography) the clouds increase in the 18K experiment. The lowest panel in Fig. 11 shows that the high level (cirrus) clouds are reduced substantially in the 18K simulation, presumably due to the reduction of penetrating moist convec-

tion and its associated transport of moisture. Most of these changes are consistent with those in the doubled CO_2 experiment, the cloud changes at 18K being the opposite of those which occur for the warmer doubled CO_2 climate.

Summary. The global mean surface air cooling of the Wisconsin ice age (compared to today) is computed from the CLIMAP boundary conditions to be ~4°C. Thus the mean temperature change between 18K and today is very similar to the projected warming for doubled CO_2. Below we analyze the contributions of different feedback processes to this global climate change.

18K Feedback Factors

We perform two types of experiments to study the feedback processes at 18K. In experiments of the first type, a given factor is modified (say the sea ice cover is changed) and the model is run for several years with the atmosphere free to adjust to the change, but with the ocean temperature and other boundary conditions fixed. Thus the only substantial feedback factors allowed to operate are water vapor and clouds (snow over land and ice can also change, but this represents only a small part of the ice/snow feedback). Experiments of this type enable us to relate surface temperature changes with flux imbalances at the top of the atmosphere under conditions of radiative/dynamic equilibrium in the atmosphere. Results of this type of experiment are summarized in the first part of Table 3 (experiments 8-14) along with the 18K control run (experiment 7). The method for converting the flux imbalance at the top of the atmosphere in these experiments to gain or feedback factors is described below in conjunction with experiment 8.

Experiments of the second type [labeled with a star (*) and tabulated in the lower part of Table 3] provide a faster, but more approximate, method for evaluating feedbacks which can be applied to certain types of radiative forcing. In the starred experiments we determine the radiative forcing by changing a factor in the control run (say sea ice cover) and calculating the instantaneous change in the planetary radiation balance at the top of the atmosphere. The atmospheric temperature and other radiative constituents and boundary conditions are not allowed to change; thus no feedbacks operate in these experiments. The flux change at the top of the atmosphere, ΔF, defines a change of planetary effective temperature

$$\Delta T_e(°C) = (\sigma T_e^3)^{-1} \Delta F(W\ m^{-2}) \sim 0.27 \Delta F(W\ m^{-2}) \quad (13)$$

for T_e = 255K. This relation provides a good estimate of the no-feedback contribution to the equilibrium surface temperature change, if the radiative perturbation does not appreciably alter the vertical temperature structure. This procedure is applicable to solar flux, surface albedo and certain tropospheric gas perturbations (Hansen et al., 1982), but does not work as simply for CO_2 perturbations, because CO_2 cools the stratosphere (Fig. 4 of Hansen et al., 1981).

Although (13) provides a useful estimate of the (no feedback) surface temperature change resulting from a given radiative imbalance at the top of the atmosphere, it is a rough estimate because the radiation to space comes from a broad range of wavelengths and altitudes. In order to account for this spectral dependence, we used the 1-D radiative convective model for the following experiment. A flux of 1 W m^{-2} was arbitrarily added to the ocean surface, and the lapse rate, water vapor and other radiative constituents were kept fixed. The surface temperature increase at equilibrium was 0.29°C, implying

$$\Delta T_s(°C) \sim 0.29\ \Delta F(W\ m^{-2}) . \quad (14)$$

The coefficient in (14) is preferable to that in (13), for radiative perturbations which uniformly affect surface and atmospheric temperatures.

Water vapor and cloud feedbacks. Although we do not have measurements of the water vapor and cloud distribution for 18K, we can use experiment 8 to determine the combined water vapor/cloud feedback factor in our 3-D model for the 18K simulation. In this experiment the ocean surface temperature was arbitrarily decreased by 2°C everywhere. As shown in Table 3, the global mean surface temperature decreased by 2°C and the net radiation flux to space decreased by 2.7 W m^{-2}. Thus, with the sea ice and land ice fixed, the model sensitivity $\Delta T/\Delta F$ for the combined water vapor and cloud feedbacks is 0.76°C $(W/m^{-2})^{-1}$. If no feedbacks were allowed to operate, the sensitivity would be ~0.29°C $(W/m^2)^{-1}$, cf. equation (14). Thus, since the atmospheric feedbacks are the only ones allowed to operate in experiment 8, we infer that the combined water vapor and cloud feedback factor in our model for 18K is $f_{wc} \sim 2.6$ and $g_{wc} \sim 0.6$. This is practically the same as the combined water vapor and cloud feedbacks for the doubled CO_2 experiment [Table 1 and equation (12)].

Experiment 8 can be used to convert the flux imbalances at the top of the atmosphere in the other unstarred experiments in Table 3 to equilibrium surface temperature changes. Thus, if the ocean temperature were free to change and water vapor and clouds were the only operative feedbacks, a flux imbalance ΔF at the top of the atmosphere would vanish as the surface temperature changed by an amount $\Delta T = 0.76\ \Delta F$.

Sea ice and land ice feedbacks. Experiments 9 and 10, in which the 18K distributions of sea ice and land ice were replaced with today's distributions, show that both the sea ice and land ice changes made major contributions to the ice age cooling (Table 3). The CLIMAP sea ice and land ice distributions each affect the global ground albedo by ~0.02. Atmospheric shielding and zenith angle effects reduce the impact on plane-

TABLE 3. Changes in planetary radiation balance in climate model experiments. The control run for experiments 7, 11, and 13 is climate model II documented in paper 1. σ is the standard deviation of the annual mean about the 5 year mean for this control run; standard deviations for the other control runs were of similar magnitude. Experiment 7 was run for 6 years, with the results averaged over the final 5 years. The other unstarred experiments were run for 4 years and averaged over the final 3 years. The starred experiments were run for 3 years and averaged over 3 years. T_s is surface air temperature, F net radiation at the top of the atmosphere, A_g ground albedo and A_p planetary albedo. Global values are shown, with the numbers in parenthesis being the results for the Northern Hemisphere and Southern Hemisphere respectively. Experiment 7', the control run for experiment 12, was identical to experiment 7 except that the Koppen vegetation of Fig. 12(a) was substituted for Matthews (1983) 1° x 1° vegetation used in model II.

Experiment	Description	Control Run	ΔT_s(°C)	$100\times\Delta A_g$	$100\times\Delta A_p$	ΔF (W m^{-2})
7	18K boundary conditions	model II (paper 1)	-3.6(-4.6,-2.5)	4.1(5.0,3.1)	1.9(2.2,1.6)	-1.6(-0.1,-3.2)
8	ocean temperature reduced by 2°C	experiment 7	-2.0(-2.0,-2.0)	0.4(0.4,0.4)	0.5(0.5,0.5)	2.7(2.7,2.6)
9	today's sea ice	experiment 7	0.6(0.5,0.7)	-1.8(-0.9,-2.7)	-0.6(-0.3,-0.8)	1.7(0.6,2.8)
10	today's land ice	experiment 7	0.9(1.7,0.1)	-1.9(-3.6,-0.2)	-0.9(-1.3,-0.5)	1.9(2.4,1.4)
11	reduced 18K sea ice	model II (paper 1)	-3.5(-4.6,-2.4)	3.7(5.0,2.4)	1.8(2.2,1.4)	-1.4(0.1,-2.9)
12	18K vegetation	experiment 7'	-0.1(-0.3,0.0)	0.6(1.2,0.0)	0.3(0.5, 0.1)	-0.9(-1.4,-0.4)
13	modified 18K boundary conditions	model II (paper 1)	-3.7(-5.0,-2.4)	3.4(4.9,1.9)	1.7(2.2,1.3)	-2.1(-0.2,-3.9)
14	CO_2 (315→200 ppm)	experiment 7	-0.2(-0.3,-0.1)	0.1(0.1,0.1)	0.2(0.2,0.1)	-2.2(-2.3,-2.1)
9*	today's sea ice	experiment 7	-	-1.6(-0.8,-2.6)	-0.5(-0.4,-0.7)	3.1(2.0,4.3)
10*	today's land ice	experiment 7	-	-1.5(-2.7,-0.4)	-0.6(-1.1,0.0)	3.6(6.4,0.7)
11*	today's sea ice	experiment 11	-	-1.3(-0.9,-1.8)	-0.5(-0.4,-0.6)	2.6(1.8,3.3)
	$\sigma_{control}$		0.04(0.03,0.06)	0.05(0.07,0.03)	0.09(0.09.0.10)	0.3(0.3,0.4)

tary albedo to 0.006 for the sea ice change and 0.009 for the land ice change. The impact on the net radiation balance with space is between 1.5 and 2.0 W m^{-2} in each case, for these experiments in which the atmosphere was allowed to adjust to the changed sea ice and land ice.

The radiation imbalances in these experiments of the first type can be used to estimate the gain factors for these two feedback processes. Based on the conversion factor 0.76°C/(W m^{-2}), the flux imbalances in experiments 9 and 10 yield equilibrium surface temperature changes of $\Delta T_{sea\ ice}$ = 1.9K and $\Delta T_{land\ ice}$ = 2.3K. Since the feedback factor in these experiments is f_{wc} = 2.6, the radiative forcings produced by the sea ice and land ice changes in the absence of feedbacks are $\Delta T_{sea\ ice} = 1.9K/f_{wc} = 0.7K$ and $\Delta T_{land\ ice}$ = 0.9K, respectively. Thus the gain factors for sea ice and land ice changes, for the climate change from 18K to today, can be estimated as

$$g_{sea\ ice} \sim 0.7/\Delta T \sim 0.14\text{-}0.20$$
$$g_{land\ ice} \sim 0.9/\Delta T \sim 0.18\text{-}0.25 , \quad (15)$$

where ΔT is the change of global mean surface air temperature in °C between 18K and today. Experiment 7 yields ΔT = 3.6°C, but indications that CLIMAP low latitude ocean temperatures are too warm (see above) suggest $\Delta T \sim 5°C$; the range given for g refers to ΔT = 3.6-5°C.

In experiments 9* and 10* the 18K distributions of sea ice and land ice in experiment 1 were replaced with today's distributions, but only for diagnostic calculation of the planetary radiation balance; all other quantities in the diagnostic calculation were from experiment 7. Based on the radiative forcings computed at the top of the atmosphere and Eq. (13) we estimate the gain factors, $g_i = \Delta T_i/\Delta T$, for the sea ice and land ice changes to be

$$g_{sea\ ice} \sim \frac{0.27 \times 3.1}{\Delta T} \sim 0.17\text{-}0.23$$
$$g_{land\ ice} \sim \frac{0.27 \times 3.6}{\Delta T} \sim 0.19\text{-}0.27 . \quad (16)$$

These gain factors include the effect of ice on thermal emission and planetary albedo. The fact that the gains estimated from (16) exceed those from (15) indicates that the emission from the added snow and ice surfaces on the average is from a somewhat higher temperature than the effective temperature, 255K.

The accuracy of these feedback gains depends primarily on the accuracy of the CLIMAP boundary conditions. Indeed, it is possible that the CLIMAP sea ice distribution is too extensive. Burckle et al. (1982), on the basis of satellite measurements of sea ice coverage and present sediment distributions, suggest that the sediment boundaries which CLIMAP had assumed to be the summer sea ice limit in the Southern Hemisphere are in fact more representative of the spring sea ice limit. Experiments 11 and 11* test the effect of this reduced sea ice coverage. In experiment 1 the CLIMAP February and August sea ice coverage were used as the extremes and interpolated sinusoidally to other months. For experiments 11 and 11* the winter (August) coverage was left unchanged, but the CLIMAP Southern Hemisphere February coverage was used for the spring (November) with linear extrapolation to February, and linear interpolation between the February and August extremes.

Experiment 11* implies that the sea ice gain estimated in experiments 9 and 9* should be reduced by 15-20 percent, if the arguments of Burckle et al. (1982) are correct. Although there is uncertainty about the true 18K sea ice distribution, it seems likely that the original CLIMAP data is somewhat an overestimate. On the basis of experiments 9, 9* and 11* our best estimate of the sea ice gain for the climate change from 18K to today is $g_{sea\ ice} \sim 0.15$ and thus a feedback factor $f_{sea\ ice} \sim 1.2$. This is larger than the snow/ice feedback obtained in the S_o and CO_2 experiments. However, the area of the sea ice cover change is about twice as large in the 18K experiment (-18.4×10^6 km^2 for the annual mean with our revised CLIMAP sea ice) than in these other experiments (7.8×10^6 km^2, 9.2×10^6 km^2 and 14.8×10^6 km^2 in the S_o, CO_2 and alternate CO_2 experiments, respectively). Thus, the gains obtained from the ice age and the warmer climate experiments are consistent.

It also has been argued (DiLabio and Klassen, 1983) that the CLIMAP land ice cover is an overestimate, because the ice sheet peripheries probably did not all achieve maximal extent simultaneously. This possibility was recognized by the CLIMAP investigators, who therefore also presented a minimal extent ice sheet model for 18K (Denton and Hughes, 1981; CLIMAP, 1981). In this minimal ice model the area by which the ice sheets of 18K exceeded those of today is reduced to five-sixths of the value in the standard CLIMAP model. We conclude that the land ice gain for the climate change from 18K to today is 0.15-0.25. The corresponding feedback factor is 1.2-1.3.

Vegetation feedback. We also investigated the vegetation feedback, which Cess (1978) has estimated to provide a large positive feedback. We used the Koppen (1936) scheme, which relates annual and monthly mean temperature and rainfall to vegetation type, to infer expected global vegetation distributions for the GCM runs representing today's climate (model II in paper 1) and the 18K climate. The resulting vegetation distribution from the run with today's boundary conditions (Fig. 12a) suggests that the model and Koppen scheme can do a fair job of 'predicting' vegetation, in the case of today's climate for which the scheme was derived. Discrepancies with observed vegetation (Matthews, 1983) exist, e.g.,

there is too much rainforest on the east coast of Africa and too little boreal forest in central Asia, but the overall patterns are realistic.

The vegetation distribution obtained for 18K (Fig. 12b) from the Koppen scheme and our 18K experiment has more desert than today, less rainforest and less boreal forest. These changes are qualitatively consistent with empirical evidence of tropical aridity during the last glacial maximum based on a variety of paleoclimate indicators, such as pollen (Flenley, 1979), fauna (Vuilleumier, 1971), geomorphology (Sarnthein, 1978) and lake levels (Street and Grove, 1979). However, the magnitude of the desert and rainforest changes is smaller than suggested by the paleoclimate evidence. The smaller changes may result from (a) the CLIMAP tropical ocean temperatures being too warm, as discussed above, which would tend to cause an overestimate of rainforest and underestimate of desert area; (b) the lower atmospheric CO_2 abundance of 18K (Shackleton et al., 1983), since CO_2 'fertilization' effects are not included in the Koppen scheme.

In experiment 12 today's vegetation was replaced with the Koppen 18K vegetation (Fig. 12b). The land, land ice and other boundary conditions were identical to those in the control run. In this experiment the modified vegetation directly affects the planetary albedo and also indirectly affects it through the masking depth for snow (paper 1). The 18K Kopppen vegetation of Fig. 12b increased the global ground albedo by 0.006 and the planetary albedo by 0.003 (Table 3) and left a flux imbalance of -0.9 W m^{-2} at the top of the atmosphere. Based on the same analysis as for ice above, the no-feedback temperature change due to vegetation is 0.3°C, yielding $g_{vegetation}$ = 0.06-0.08. Because of the imprecisions in the Koppen 18K vegetation, we broaden the estimated gain to $g_{vegetation}$ = 0.05-0.09, and thus $f_{vegetation}$ = 1.05-1.1. Examination of global maps shows that the greatest impact of the changed vegetation was the replacement of European and Asian evergreen forests with tundra and grassland; the greatly reduced masking depths produced annual ground albedo increases of 0.1 or more over large areas, with the largest changes in spring. For reasons stated above, we also examined an 18K run with ocean temperatures reduced by 2°C; this reduced the number of gridboxes with rainforest from 10 to 5 in South America and from 7 to 2 in Africa, compared to Fig. 12b, in better agreement with paleoclimate evidence cited above. This additional vegetation change did not significantly change the global albedo or flux at the top of the atmosphere.

We conclude that the vegetation feedback factor between 18K and today is $f_{vegetation}$ ~ 1.05-1.1. This is much smaller than suggested by Cess (1978), but consistent with the analysis of Dickinson (1984). We find a somewhat larger feedback than Dickinson obtained, 0.003 change of planetary albedo compared to his 0.002, apparently due to the change of vegetation masking of snow-covered ground.

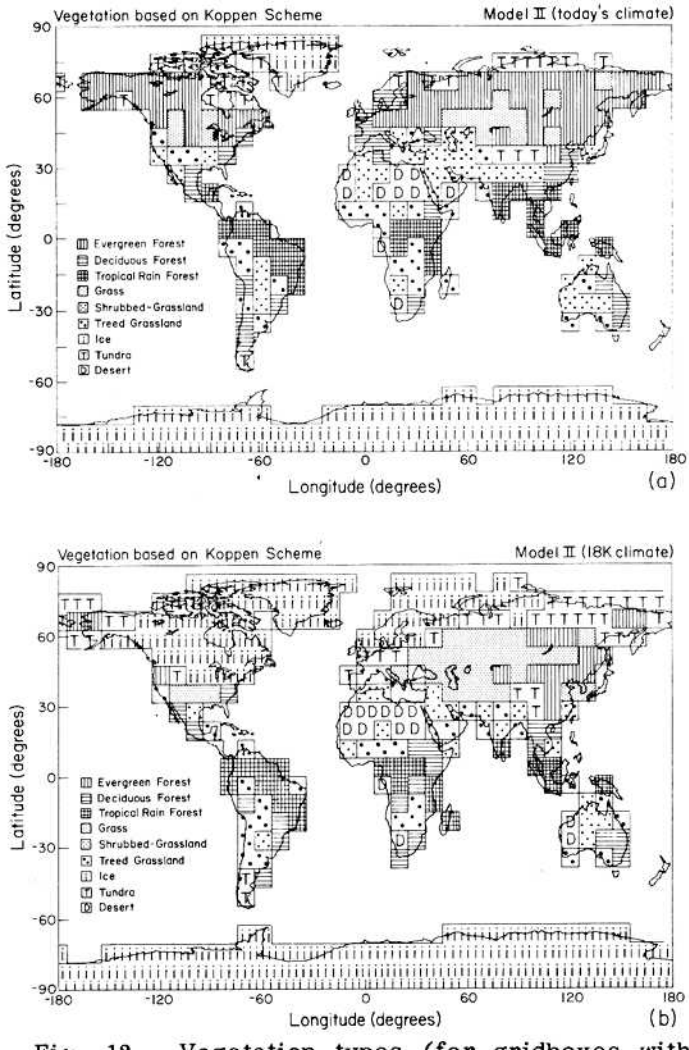

Fig. 12. Vegetation types (for gridboxes with more than 30 percent land) inferred from 3-D model simulations and the Koppen (1936) scheme, which relates annual and monthly mean temperature and precipitation to vegetation type. (a) is the control run for today's climate (paper 1), while (b) is the 18K simulation (experiment 7).

18K Radiation Balance

The simulated 18K climate (experiment 7) is close to radiation balance, the imbalance (Table 3) being 1.6 W m^{-2} at the top of the atmosphere, compared to the control run (model II) for today's climate. This imbalance is small compared to the amount of solar energy absorbed by the planet (~240 W m^{-2}). However, in reality even more precise radiation balance must have existed averaged over sufficient time, because the ice age lasted much longer than the thermal relaxation time of the ocean. (Melting the ice sheets in 10K years would require a global mean imbalance of only ~0.1 W m^{-2}.) Although the model calculations contain imprecisions comparable in magnitude to the radiation imbalance, we expect these to be largely cancelled by the procedure of differencing

with the control run. This type of study should become a powerful tool in the future, as the accuracy of the reconstructed ice age boundary conditions improves and as the climate models become more realistic.

Taken at face value, the radiation imbalance in the 18K experiment 7 implies an imprecision in either some of the assumed boundary conditions for 18K or in the climate model sensitivity. The sense of the imbalance is such that the planet would cool further (to -4.8°C, based on the ΔF in Table 3), if the ocean temperature were computed rather than specified. Before studying this imbalance further, we make three modifications to the 18K simulation. First, the Southern Hemisphere sea ice cover is reduced as discussed above; this reduces the radiation imbalance. Second, the vegetation is replaced by the 18K vegetation of Fig. 12b; this slightly reduces the radiation imbalance. Third, the amount of atmospheric CO_2 is reduced in accord with evidence (Neftel et al., 1982) that the 18K CO_2 amount was only ~200 ppm; this significantly aggravates the radiation imbalance.

These three changes are all included in experiment 13, the sea ice and vegetation changes being those tested in experiments 11 and 12. The CO_2 decrease was 75 ppm from the control run value of 315 ppm; this is equivalent to the change from an estimated preindustrial abundance of 270 ppm to an ice age abundance of ~200 ppm. With these changes the radiation imbalance with space becomes 2.1 W m^{-2}. This imbalance would carry the surface temperature to -5.3°C if the constraint on ocean temperature were released.

Two principal candidates we can identify for redressing the 18K radiation imbalance are the CLIMAP sea surface temperatures and the cloud feedback in the climate model. The imbalance is removed if the CLIMAP ocean temperature is 1.5°C too warm (experiment 8, Table 3). The possibility that the CLIMAP sea surface temperatures may be too warm is suggested by the discussion above. The imbalance is also removed if it is assumed that clouds provide no feedback, rather than the positive feedback which they cause in this model; this conclusion is based on the estimate that the clouds cause 30-40 percent of the combined water vapor/cloud feedback (experiment 8), as is the case in the S_0 and CO_2 experiments.

One plausible solution is the combination of a reduction of low latitude ocean temperature by ~1°C and a cloud feedback factor between 1 and 1.3. An alternative is a reduction of low latitude ocean temperature by ~1°C and a greater value for the 18K CO_2 abundance; indeed, recent analyses of Shackleton et al. (1983) suggest a mean 18K CO_2 abundance ~240 ppm. It is also possible that there were other presently unsuspected changes of boundary conditions.

There are presently too many uncertainties in the climate boundary conditions and climate model to permit identification of the cause of the radiation imbalance in the 18K simulation. However, as the boundary conditions and climate models become more accurate, this approach should yield valuable checks on paleoclimate data and climate models. In the meantime, the data permits some general conclusions about the strength of climate feedback processes.

Conclusions from 18K Experiments

The above calculations suggest the following major contributions to the global cooling at 18K, as shown schematically in Fig. 13:

$$\Delta T_{\text{water vapor + clouds}} \equiv \Delta T_{wc} \sim 1.4\text{-}2.2°C$$

$$\Delta T_{\text{land ice}} \equiv \Delta T_l \sim 0.7\text{-}0.9°C$$

$$\Delta T_{\text{sea ice}} \equiv \Delta T_s \sim 0.6\text{-}0.7°C \qquad (17)$$

$$\Delta T_{CO_2} \sim 0.3\text{-}0.6°C$$

$$\Delta T_{\text{vegetation}} \equiv \Delta T_v \sim 0.3°C$$

These estimates are the product of the gain for each process and the total cooling at 18K. But note that the uncertainty in the total ΔT cancels in obtaining ΔT_l, ΔT_s, ΔT_{CO_2} and ΔT_v; thus these ΔT_i are more fundamental and accurate than the corresponding g_i. The ΔT_i represent the isolated radiative forcings, which can be computed accurately, for the assumed changes in these radiative constituents between 18K and today. $\Delta T_{wc} = 2.2°C$ is obtained from experiment 8 which yielded $g_{wc} \sim 0.6$. The cloud portion of ΔT_{wc} is uncertain because of the rudimentary state of cloud modeling; however even with no cloud feedback the water vapor contribution (~1.4°C) is a large part of the total ice age cooling. $\Delta T_l = 0.9°C$ is based on the CLIMAP maximal ice sheet extent; it is ~0.7°C for the minimal extent model. $\Delta T_s = 0.7°C$ is based on CLIMAP sea ice; it is 0.6°C with the reduced sea ice cover in the Southern Hemisphere in experiments 11 and 11*. $\Delta T_{CO_2} = 0.6°C$ refers to a CO_2 change from 200 ppm (at 18K) to 300 ppm (at say 1900); this is reduced to 0.3°C if the CO_2 amount was 225 ppm at 18K and 275 ppm at 1900.

The sum of the temperature contributions in Fig. 13 slightly exceeds the computed cooling ΔT = 3.7°C at 18K. This is a restatement of the radiation imbalance which exists in the model when the CLIMAP boundary conditions are used with ΔCO_2 of 50-100 ppm. If the model ocean temperature were allowed to change to achieve radiation balance, it would balance at a global mean 18K cooling of ~5.3°C [model sensitivity = 0.76°C/(W m^{-2})]. We conclude that either the CLIMAP 18K ocean temperatures are too warm by ~1.5°C or we have overestimated one or more of the contributions to the 18K cooling in (17).

It is apparent from Fig. 13 that feedback processes account for most of the 18K cooling. The

water vapor, cloud and sea ice contributions represent at least half of the total cooling. On long time scales the land ice portion of the cooling also may be regarded as a feedback, though it operates on a very regional scale and may be a complex function of a variety of factors such as the position of land areas, ocean currents and the meteorological situation. Even the CO_2 portion of the cooling, or at least part of it, may be a feedback, i.e., in response to the change of climate.

Variations in the amount of absorbed solar radiation due to Milankovitch (earth orbital) changes in the seasonal and latitudinal distributions of solar irradiance, which occur on time scales of several thousand years, can provide a global mean forcing of up to a few tenths of a degree. In view of the strength of the climate feedbacks, it is plausible for the Milankovitch and CO_2 forcings to 'drive' glacial to interglacial climate variations. However, discussion of the sequence of causes and mechanisms of glacial to interglacial climate change is beyond the scope of this paper.

We can use the contributions to the 18K cooling summarized in Fig. 13 to obtain an empirical estimate of the climate feedback factor due to the processes operating on 10-100 year time scales, taking the land ice, CO_2 and vegetation changes from 18K to today as slow (or at least specified). The global mean radiative forcing due to the difference in 18K and today's orbital parameters is negligible compared to the other forcing summarized in Fig. 13. The feedback factor for the fast (water vapor, clouds, sea ice) processes is

$$f(\text{fast processes}) = \frac{\Delta T(\text{total})}{\Delta T(\text{slow processes})} \qquad (18)$$

$\Delta T(\text{total})$ is ~3.7°C for the CLIMAP boundary conditions, but may be ~5°C, if CLIMAP low latitude ocean temperatures are 1-2°C too warm. Using the nominal CLIMAP boundary conditions and intermediate estimates for $\Delta T_l \sim 0.4$, $\Delta T_{CO_2} \sim 0.45$ and $\Delta T_v \sim 0.3$, yields f(fast processes) ~ 2.4. Using $\Delta T(\text{total}) \sim 5°C$ and these nominal radiative forcings yields $f \sim 3.2$. Allowing for the more extreme combinations of the forcings and $\Delta T(\text{total})$, we conclude that

$$f(\text{fast processes}) \sim 2\text{-}4 \qquad (19)$$

This feedback factor, f ~ 2-4, corresponds to a climate sensitivity of 2.5-5°C for doubled CO_2. Note that this result is independent of our climate model sensitivity: it depends on the total ΔT at 18K (fixed by CLIMAP) and on the assumption that land ice, CO_2 and vegetation are the only major slowly changing boundary conditions. Of course some vegetation and CO_2 feedbacks may occur in less than 100 years but for projecting future climate it is normal to take these as specified boundary conditions.

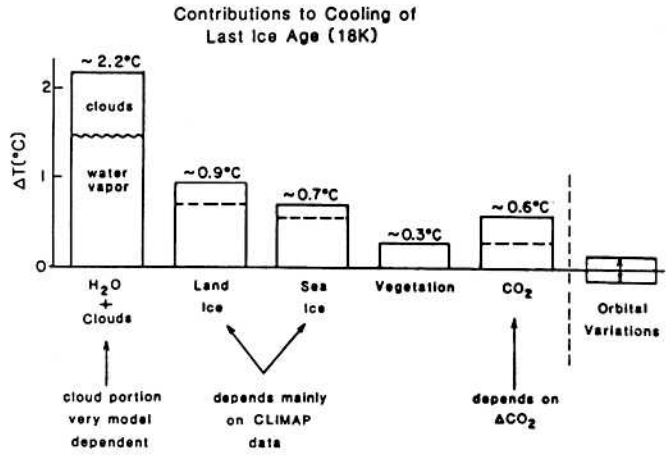

Fig. 13. Contributions to the global mean temperature difference between the Wisconsin ice age and today's climate as evaluated with a 3-D climate model and assumed boundary conditions. The cloud and water vapor portions were not separated, but based on other 3-D experiments the cloud part is estimated as 30-40 percent of their sum. The dashed line for land ice refers to the 'minimal extent' model of CLIMAP, and the dashed line for sea ice refers to the reduced sea ice cover discussed in the text. The solid line for CO_2 refers to $\Delta CO_2 \sim 100$ ppm (300 ppm → 200 ppm) and the dashed line to $\Delta CO_2 \sim 50$ ppm.

Finally, note that a given sensitivity for fast feedback processes, say 4°C for doubled CO_2, does not mean that the climate necessarily would warm by 4°C in 10 or even 100 years. Although water vapor, cloud and sea ice feedbacks respond rapidly to climate change, the speed of the climate response to a changed forcing depends on the rate at which heat is supplied to the ocean and on transport processes in the ocean.

Transient Response

Surface Response Time

The time required for the surface temperature to approach its new equilibrium value in response to a change in climate forcing depends on the feedback factor, f. The following example helps clarify this relationship.

Let the solar flux absorbed by a simple blackbody planet ($f \equiv 1$) change suddenly from $F_0 = \sigma T_0^4$ to $F_0 + \Delta F \equiv \sigma T_1^4$, with $\Delta F \ll F_0$. The rate of change of heat in the climate system is

$$\frac{d(cT)}{dt} = \sigma T_1^4 - \sigma T^4 \sim -4\sigma T_0^3 (T - T_1) \qquad (20)$$

where c is the heat capacity per unit area and T is the time varying temperature. Since $T_1 - T_0 \ll T_0$, the solution is

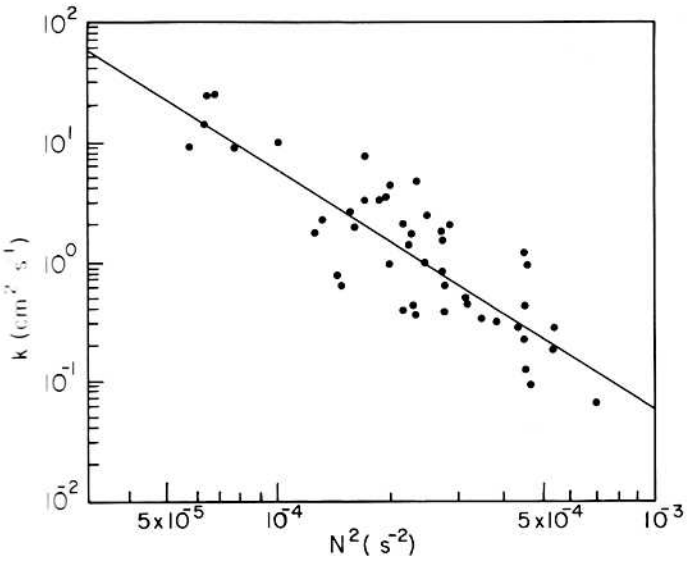

Fig. 14. Relationship between the effective diffusion coefficient (k) and the stability (N^2, where N is the Brunt-Vaisala frequency) at the base of the winter mixed layer for the GEOSECS tritium stations north of 20°S. The regression line fit (Eq. 25) has correlation coefficient 0.85 with the points for individual stations.

$$T - T_o = (T_1 - T_o)[1 - \exp(-t/\tau_b)] \qquad (21)$$

where the blackbody no-feedback e-folding time is

$$\tau_b = c/4\sigma T_o^3 \ . \qquad (22)$$

For a planet with effective temperature 255 K and heat capacity provided by 63m of water (as in our 3-D experiments), τ_b is approximately 2.2 years. Thus, this planet with f = 1 exponentially approaches its new equilibrium temperature with e-folding time 2.2 years.

Feedbacks modify the response time since they come into play only gradually as the warming occurs, the initial flux of heat into the ocean being independent of feedbacks. It is apparent that the actual e-folding time for a simple mixed layer heat capacity is

$$\tau = f\tau_b \qquad (23)$$

An analytic derivation of (23) is given in Appendix A. The proportionality of the mixed layer response time to f is apparent in Fig. 3; the e-folding time for that model, which has f ~ 3.5 and a 63m mixed layer, is ~8 years.

The 63m mixed layer depth in our 3-D experiments was chosen as the minimum needed to obtain a realistic seasonal cycle of temperature, thus minimizing computer time needed to reach equilibrium. However, the global-mean annual-maximum mixed layer depth from our compilation of observations (see above) is ~110m, and thus the isolated ocean mixed layer has a thermal response time of ~15 years if the climate sensitivity is 4°C for doubled CO_2. Even if the climate sensitivity is 2-3°C for doubled CO_2, the (isolated) mixed layer response time is about 10 years.

In order to determine the effect of deep ocean layers on the surface response time, it is useful to express the heat flux into the ocean as a function of the difference between current surface temperature and the equilibrium temperature for current atmospheric composition. In Appendix A we show that

$$F(W\ m^{-2}) = \frac{F_o}{\Delta T_{eq}(2*CO_2)} \ (\Delta T_{eq} - \Delta T) \qquad (24)$$

where ΔT is the ocean surface temperature departure from an arbitrary reference state and ΔT_{eq} is the equilibrium temperature departure for current atmospheric composition. $\Delta T_{eq}(2*CO_2)$ is the equilibrium sensitivity for doubled CO_2; for our 3-D climate model it is 4.2°C. F_o is the flux into the ocean in the model when CO_2 is doubled and the stratospheric temperature has equilibrated; our 3-D model yields F_o = 4.3 W m^{-2}.

The long response time of the isolated mixed layer allows a portion of the thermal inertia of the deeper ocean to come into play in delaying surface temperature equilibrium. Exchange between the mixed layer and deeper ocean occurs by means of convective overturning in the North Atlantic and Antarctic oceans and principally by nearly horizontal motion along isopycnal (constant density) surfaces at lower latitudes. Realistic modeling of heat perturbations is thus rather complex, especially since changes of surface heating (and other climate variables) may alter the ocean mixing. However, we can obtain a crude estimate for the surface response time by assuming that small positive heat perturbations behave as a passive tracer; numerical experiments of Bryan et al. (1984) support this assumption. Measurements of transient tracers in the ocean, such as the tritium sprinkled on the ocean surface by atmospheric atomic testing, provide a quantitative indication of the rate of exchange of water between the mixed layer and the upper thermocline (see, e.g., Ostlund et al., 1976).

We estimate an effective thermocline diffusion coefficient (k) at each GEOSECS measurement station from the criterion that the modeled and observed penetration depths (Broecker et al., 1980) be equal at each station. The resulting diffusion coefficients are well correlated (inversely) with the stability at the base of the winter mixed layer (Fig. 14). In particular, we find a correlation coefficient of 0.85 between k and $1/N^4$, where N is the Brunt-Vaisala frequency at the base of the mixed layer. The global distribution of N^2 was obtained from the ocean data set of Levitus (1982).

The empirical relation between k and stability,

$$k = 5 \times 10^{-8}/N^4, \qquad (25)$$

and the global ocean data set of Levitus (1982) yield the global distribution of k at the base of the mixed layer shown in Fig. 15a. There is a low rate of exchange ($k < 0.2$ cm^2 s^{-1}) in the eastern equatorical Pacific where upwelling and the resulting high stability at the base of the mixed layer inhibit vertical mixing, but rapid exchange ($k > 10$ cm^2 s^{-1}) in the Greenland - Norwegian Sea area of convective overturning.

The e-folding time for the mixed layer temperature (time to reach 63 percent of the equilibrium response) is shown in Fig. 15b. This is calculated from the geographically varying k and annual-maximum mixed layer depth, assuming a sudden doubling of CO_2 and an equilibrium sensitivity of 4.2°C everywhere. The (63 percent) response time is about 20-50 years at low latitudes, where the shallow mixed layer and small k allow the mixed layer temperatures to come into equilibrium relatively quickly. At high latitudes, where the deep winter mixed layer and large k result in a larger thermal inertia, the response time is about 200-400 years. The time for the global area-weighted mixed layer temperature to reach 63 percent of its equilibrium response is 124 years.

We estimate an equivalent k for use in a global 1-D model by choosing that value of k which fits the global (area-weighted) mean perturbation of the mixed layer temperature as a function of time obtained with the above calculation in which k and mixed layer depth vary geographically. We find that $k \sim 1$ cm^2 s^{-1} provides a reasonable global fit to the area-weighted local calculations for either a step function change of CO_2 or exponentially increasing CO_2 amount. Other analyses of the tracer data yield empirical values of 1-2 cm^2 s^{-1} for the effective rate of exchange between the mixed layer and deeper ocean (Broecker et al., 1980).

The delay time due to the ocean thermal inertia is graphically displayed in Fig. 16. Equation (24) provides a good approximation of the time dependence of the heat flux into the ocean in our 3-D climate experiment with doubled CO_2, as shown by comparison of Figs. 3b and 16. Note that in our calculation with a mixed layer depth of 110 m, $k = 1$ cm^2 s^{-1}, and $\Delta T_{eq} = 4.2$°C. The time required to reach a response of 2.65°C is 102 years. This is in rough agreement with the 124 years obtained above with the 3-D calculation.

The ocean delay time is proportional to f for an isolated mixed layer [eq. (23) and Appendix A], but depends more strongly on f if mixing into the deeper ocean is included. Our 1-D calculation with $k = 1$ cm^2 s^{-1} and mixed layer depth 110 m yields an e-folding time of 55 years for $\Delta T_{eq} = 3$°C and 27 years for $\Delta T_{eq} = 2$°C. Thus our ocean response time is consistent with that of Bryan et al. (1982), who obtained a response time of about 25 years for a climate model with sensitivity ~2°C for doubled CO_2.

Although our calculations were made with a simple diffusion model, the conclusion that the ocean surface temperature response time is highly nonlinear in ΔT_{eq} (or f) is clearly more general. The surface response time increases faster than linearly with f when the deeper ocean is included, because as f increases greater ocean depths come into play. Thus more realistic modeling of ocean transport processes should not modify these conclusions for small climate perturbations.

Our calculations of ocean response time neglect ocean circulation feedbacks on climate. The relationship between k and stability, equation (25), provides one way to examine the temperature feedback. By using that relation with

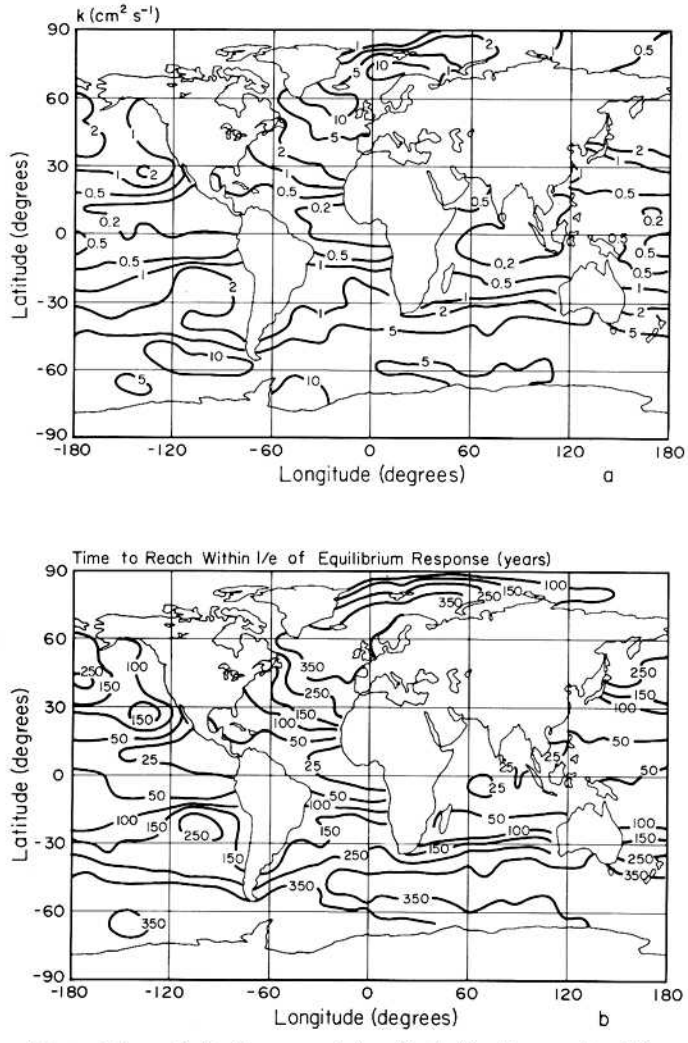

Fig. 15. (a) Geographic distribution of effective thermocline diffusion coefficient, k ($cm^2 s^{-1}$). k is derived from Eq. 25 and the global distribution of N^2, the latter obtained from the ocean data of Levitus (1982). (b) Geographic distribution of the 63 percent response time for surface temperature response to doubled CO_2 in the atmosphere. Only geographic variability of k and mixed layer depth are accounted for. $\Delta T_{eq}(2*CO_2)$ is taken as 4.2°C everywhere. The flux into the ocean is from Eq. (24).

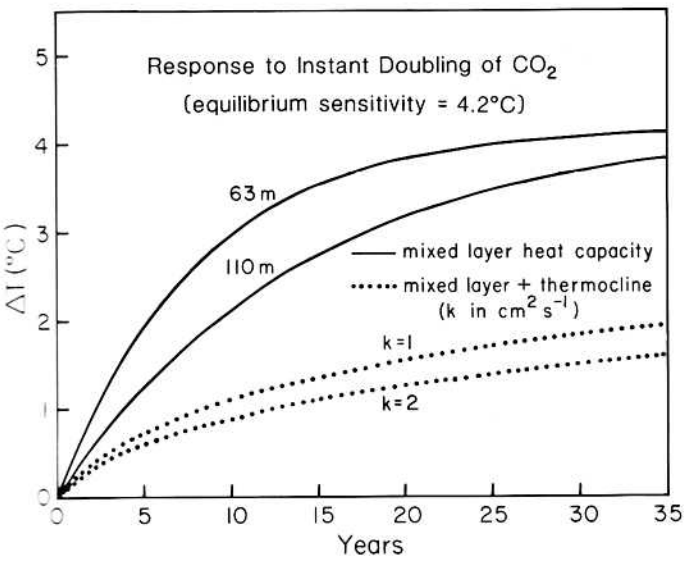

Fig. 16. Transient response to step function doubling of atmospheric CO_2 from 315 ppm to 630 ppm, computed from (24) with three representations of the ocean. The 63 m mixed layer corresponds to the mean mixed layer depth in the 3-D experiments; 110 m is the global-mean annual maximum mixed layer depth obtained from global ocean data. The curves including diffusion beneath the mixed layer are not exponentials (Appendix A).

our 1-D ocean diffusion model, we find that the time required to reach a given transient response is decreased, typically by several percent. Real ocean transports may be more sensitive to surface warming, as well as to related mechanisms such as melting of sea ice and ice sheets and changing winds, precipitation and evaporation. It is easy to construct scenarios in which the ocean feedbacks are much greater, especially in the areas of deep water formation, but not enough information is available for reliable calculation of ocean/climate feedbacks.

Finally, we note that the ocean surface thermal response time reported in the literature generally has been 8-25 years (Hunt and Wells, 1979; Hoffert et al., 1980; Cess and Goldenberg, 1981; Schneider and Thompson, 1981; Bryan et al., 1982). The 3-D ocean model result of Bryan et al. is consistent with our model when we employ a climate sensitivity of 2°C for doubled CO_2, as noted above. The discrepancy between our model response time and that of the other models arises from both the climate sensitivities employed and the choice of ocean model parameters. Key parameters are: mixed layer depth (we use 110m since any depth mixed during the year should be included), rate of exchange with deeper ocean (we use diffusion with k = 1 cm^2 s^{-1}, the minimum global value suggested by transient tracers, cf., Broecker et al., 1980) and the atmosphere-ocean heat flux [we use (24) which has initial value 4.3 W m^{-2} over the ocean area for doubled CO_2 and is consistent with other 3-D models]. Obviously the use of a 1-D box-diffusion model is a gross oversimplification of ocean transports. As an intermediate step between this and a 3-D ocean general circulation model, it may be valuable to study the problem with a model which ventilates the thermocline by means of transport along isopycnal surfaces. The agreement between the results from the 3-D ocean model of Bryan et al. and our model with a similar climate sensitivity suggests that our approach yields a response time of the correct order.

Impact on Empirically-Derived Climate Sensitivity

The delay in surface temperature response due to the ocean must be included if one attempts to deduce climate sensitivity from empirical data on time scales of order 10^2 years or less. Furthermore, in such an analysis it must be recognized that the lag caused by the ocean is not a constant, independent of climate sensitivity.

We computed the expected warming due to increase of CO_2 between 1850 and 1980 as a function of the equilibrium climate sensitivity. Results are shown in Fig. 17a for five choices of the 1850 CO_2 abundance (270±20 ppm), with CO_2 increasing linearly to 315 ppm in 1958 and then based on Keeling et al. (1982) measurments to 338 ppm in 1980. For simplicity a one-dimensional ocean was employed with mixed layer depth 110m and k = 1 cm^2 s^{-1}. However, we obtained a practically identical graph when we used a simple three-dimensional ocean with the mixed layer depth varying geographically according to the data of Levitus (1982) and k varying as in Fig. 15a.

Use of Fig. 17a is as follows. If we take 270 ppm as the 1850 CO_2 abundance (WMO, 1983) and assume that the estimated global warming of 0.5°C between 1850 and 1980 (CDAC, 1983) was due to the CO_2 growth, the implied climate sensitivity is 4°C for doubled CO_2 (f = 3-4). Results for other choices of the 1850 CO_2 abundance or global warming can be read from the figure.

Undoubtedly some other greenhouse gases also have increased in the past 130 years. Chloroflourocarbons, for example, are of recent anthropogenic origin. CH_4 and N_2O are presently increasing at rates of 1-2 percent yr^{-1} and 0.2-0.3 percent per yr^{-1}, respectively (Ehhalt, et al., 1983; Weiss, 1981; CDAC, 1983). We estimate the influence of these gases on the empirical climate sensitivity by using the trace gas scenarios in Table 4. Although the CH_4 and N_2O histories are uncertain, the chlorofluorocarbons provide most of the non-CO_2 greenhouse effect, at least in the past 10-20 years (Lacis et al., 1981), and their release rates are known. CH_4 may have increased slowly for the past several hundred years (Craig and Chou, 1982), but the reported rate of increase would not affect the results much. O_3 is also a potent greenhouse gas, but information on its past

history is not adequate to permit its effect to be included.

The climate sensitivity implied by the assumed global warming since 1850, including the effect of trace gases in addition to CO_2, is shown in Fig. 17b. If the 1850 CO_2 abundance was 270±10 ppm, as concluded by WMO (1983), a warming of 0.5°C requires a climate sensitivity 2.5-5°C for doubled CO_2. The range for the implied climate sensitivity increases if uncertainty in the amount of warming is also included. For example, a warming of 0.4-0.6°C and an 1850 CO_2 abundance of 270±10 ppm yield a climate sensitivity of 2-7°C.

Although other climate forcings, such as volcanic aerosols and solar irradiance, may affect this analysis, we do not have information adequate to establish substantially different magnitudes of these forcings prior to and subsequent to 1850.

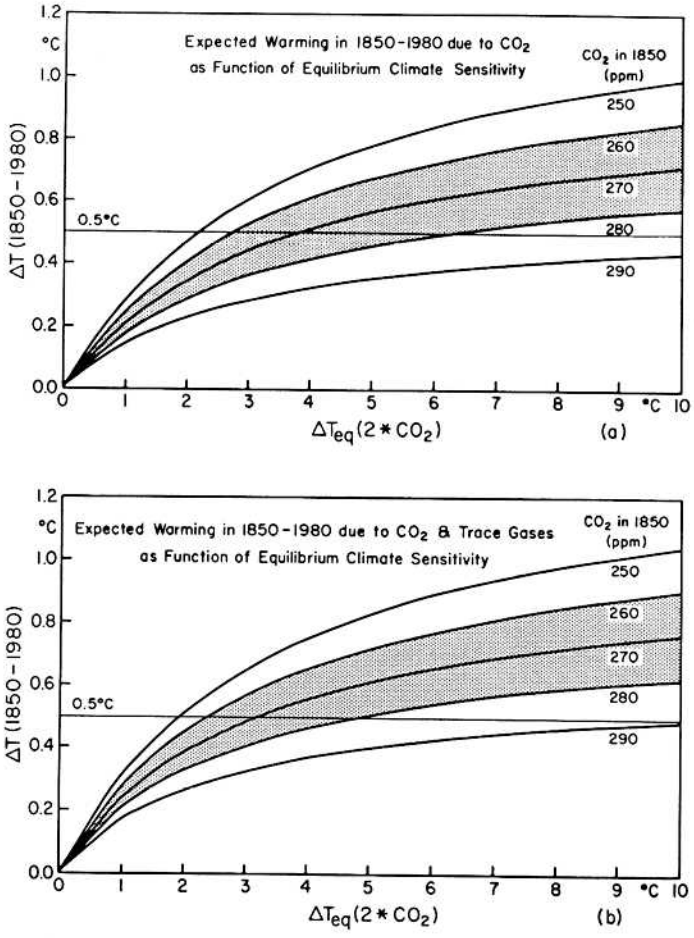

Fig. 17. Computed global warming between 1850 and 1980 as a function of the equilibrium climate sensitivity for doubled CO_2 (315 ppm → 630 ppm), $\Delta T_{eq}(2*CO_2)$. Results are shown for five values of the assumed abundance of CO_2 in 1850; the shaded area covers the range 270±10 ppm recommended by WMO (1983). (a) includes only CO_2 growth, while (b) also includes the trace gas growths of Table 4. In all cases CO_2 increases linearly from the 1850 abundance to 315 ppm in 1958 and then according to measurements of Keeling et al. (1982).

TABLE 4. Trace gas abundances employed in our calculations of the transient climate response for Figs. 17b and 18. CO_2 increases linearly for 1850-1958 and as observed by Keeling et al. (1982) for 1958-1980; ΔCO_2 increases about 2 percent yr^{-1} in the future. The chlorofluorocarbon abundances are based on estimated release rates to date, 150 year and 75 year lifetimes for CCl_2F_2 and CCl_3F, respectively, and constant future emissions at the mean release rate for 1971-1980. The CH_4 increase is about 1 percent yr^{-1} for 1970-1980 and 1.5 percent yr^{-1} after 1980. The N_2O increase is 0.2 percent yr^{-1} for 1970-1980 and 0.3 percent yr^{-1} after 1980.

Date	CO_2 (ppm)	CCl_2F_2 (ppt)	CCl_3F (ppt)	CH_4 (ppb)	N_2O (ppb)
1850	270	0	0	1400	295
1900	291	0	0	1400	295
1950	312	7	1	1400	295
1960	317	33	11	1416	295
1970	326	126	62	1500	295
1980	338	308	178	1650	301
1990	353	479	280	1815	307
2000	372	638	369	1996	313
2010	396	787	447	2196	320

The climate sensitivity we have inferred is larger than obtained by CDAC (1983) from analysis of the same time period (1850-1980) with the same assumed temperature rise. The chief reason is that CDAC did not account for the dependence of the ocean response time on climate sensitivity [equation (23) and Appendix A]. Their choice of a 15 year response time, independent of ΔT_{eq} or f, biased their result to low sensitivities.

We conclude that the commonly assumed empirical temperature increase for the period 1850-1980 (0.5°C) suggests a climate sensitivity of 2.5-5°C (f=2-4) for doubled CO_2. The significance of this conclusion is limited by uncertainties in past atmospheric composition, the true global mean temperature change and its cause, and the rate at which the ocean takes up heat. However, knowledge of these factors may improve in the future, which will make this a powerful technique for investigating climate sensitivity.

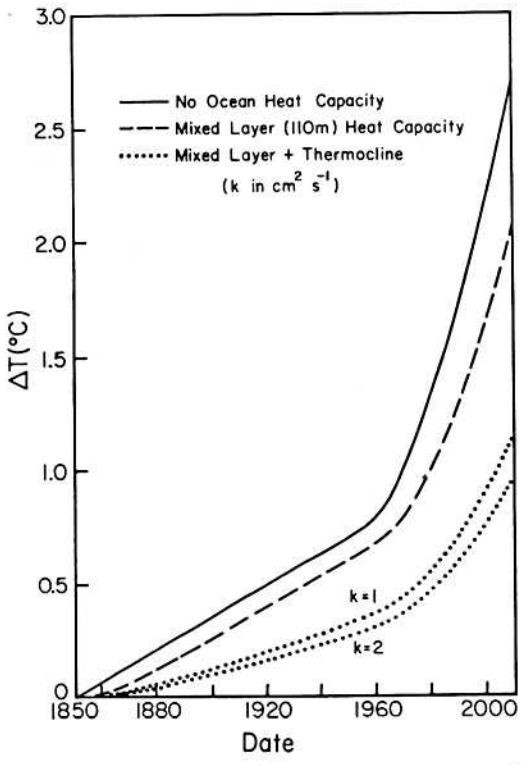

Fig. 18. Global mean warming computed for the CO_2 and trace gas scenarios in Table 4.

Growing Gap Between Current and Equilibrium Climate

One implication of the long surface temperature response time is that our current climate may be substantially out of equilibrium with current atmospheric composition, as a result of the growth of atmospheric CO_2 and trace gases during recent decades. For example, in the last 25 years CO_2 increased from 315 ppm to 340 ppm and the chloroflourocarbons from near zero to their present abundance. Since the growth rates increased during the period, the gas added during the past 25 years has been present on the average about 10 years. 10 years is short compared to the surface temperature response time, even if the climate sensitivity is only 2.5°C for doubled CO_2.

We illustrate the magnitude of this disequilibrium by making some calculations with the 1-D model specified to give the climate sensitivity of our 3-D model, 4.2°C for doubled CO_2, and with the changing atmospheric composition of Table 4. Fig. 18 shows the modeled surface temperature during the past century (1) for instant equilibrium with changing atmospheric composition, (2) with thermal lag due to the mixed layer included, and (3) with the thermocline's heat capacity included via eddy diffusion.

We infer that there is a large and growing gap between current climate and the equilibrium climate for current atmospheric composition. Based on the estimate in Fig. 18, we already have in the pipeline a future additional warming of almost 1°C, even if CO_2 and trace gases cease to increase at this time. A warming of this magnitude will elevate global mean temperature to a level at least comparable to that of the Altithermal (NAS, 1975, adapted in Fig. 1 of Hansen et al., 1984) about 6,000 years ago, the warmest period in the past 100,000 years.

The rate of warming computed after 1970 is much greater than in 1850-1980. This is because (1) ΔCO_2 is ~0.4 ppm yr^{-1} in 1850-1960, but >1 ppm yr^{-1} after 1970, and (2) trace gases, especially chlorofluorocarbons, add substantially to the warming after 1970. The surface warming computed for the period 1970-1990 is ~0.25°C; this is almost twice the standard deviation of the 5-year-smoothed global temperature (Hansen et al., 1981). But note that the equilibrium temperature increases by 0.75°C in the period 1970-1990, if the climate sensitivity is ~4°C for doubled CO_2. Thus our calculations indicate that the gap between current climate and the equilibrium climate for current atmospheric composition may grow rapidly in the immediate future, if greenhouse gases continue to increase at or near present rates.

As this gap grows, is it possible that a point will be reached at which the current climate "jumps" to the equilibrium climate? If exchange between the mixed layer and deeper ocean were reduced greatly, the equilibrium climate could be approached in as little as 10-20 years, the relaxation time of the mixed layer. Indeed, the stability of the upper ocean layers seems likely to increase as the greenhouse warming heats the ocean surface, especially if the warming leads to an increased melting of ice which adds fresh water to the mixed layer. Regions of deep-water formation, such as the North Atlantic Ocean, may be particularly sensitive to changes in surface climate. However, it is difficult to predict the net effect of greenhouse warming on ocean mixing, because changes of precipitation, evaporation and atmospheric winds, in addition to temperature, will affect ocean mixing and transport. If possible, it would be useful to examine paleoclimate records for evidence of sudden climate warmings on 10-20 year time scales, since there may have been cases in the past when the long thermal response time of the ocean allowed gaps between actual and equilibrium climates to build up.

Even if it does not lead to a dramatic jump to a new climate state, the gap between current climate and the equilibrium climate for current atmospheric composition may have important climatic effects as it grows larger. For example, it seems possible that in the summer, when zonal winds are weak, continental regions may tend partly toward their equilibrium climate, thus causing a relatively greater warming in that season. Also, in examining the climate effects of recent and future large volcanoes, such as the

1982 El Chichon eruption, the cooling effect of stratospheric aerosols must be compared to the warming by trace gases which have not yet achieved their equilibrium effect; it is not obvious that a global cooling of several tenths of a degree (Robock, 1983) should actually be expected. These problems should be studied by using a global model in which the atmospheric composition changes with time in accord with measurements, and in which the atmosphere, land and ocean each have realistic response times.

Summary

Climate Sensitivity Inferred from 3-D Models

Our analysis of climate feedbacks in 3-D models points strongly toward a net climate feedback factor of f ~ 2-4 for processes operative on 10-100 year time scales. The water vapor and sea ice feedbacks, which are believed to be reasonably well understood, together produce a feedback f ~ 2. The clouds in our model produce a feedback factor ~1.3, increasing the net feedback to f = 3-4 as a result of the nonlinear way in which feedbacks combine.

Present information on cloud processes is inadequate to permit confirmation of the cloud feedback. However, some aspects of the cloud changes in the model which contribute to the positive feedback appear to be realistic, e.g., the increase in tropical cirrus cloud cover and the increase of mean cloud altitude in conjunction with more penetrating moist convection in a warmer climate. It seems likely that clouds provide at least a small positive feedback. More realistic cloud modeling, as verified by detailed global cloud observations, is crucial for improving estimates of climate sensitivity based on climate models.

Climate Sensitivity Inferred from Paleoclimate Data

Analysis of the processes contributing to the cooling of the last ice age shows that feedbacks provide most of the cooling. The paleoclimate studies serve as proof of the importance of feedback processes and permit quantitative evaluation of the magnitude of certain feedbacks. The CLIMAP data allow us to evaluate individually the magnitudes of the land ice (f ~ 1.2-1.3) and sea ice (f ~ 1.2) feedbacks for the climate change from 18K to today, and to establish that the vegetation feedback was smaller but significant (f ~ 1.05-1.1).

We obtain an empirical estimate of f = 2.5-5 for the fast feedback processes (water vapor, clouds, sea ice) at 18K by assuming that the major radiative feedback processes have been identified (as seems likely from consideration of the radiative factors which determine the planetary energy balance with space) and grouping the slow or specified changes of the ice sheets and CO_2 as the principal climate forcings. This estimate for the fast feedback factor is consistent with the feedback in our 3-D model experiments, providing support that the model sensitivity is of the correct order.

The strength of the feedback processes at 18K implies that only relatively small climate forcings or fluctuations are needed to cause glacial to interglacial climate change. We do not try to identify the sequence of mechanisms of the glacial to interglacial changes, but it seems likely that both the direct effect of solar radiation (Milankovitch) changes on the planetary energy balance and induced changes of atmospheric composition, especially CO_2, are involved.

Climate Sensitivity Inferred from Recent Temperature Trends

The temperature increase believed to have occurred in the past 130 years (~0.5°C) implies a climate sensitivity 2.5-5°C for doubled CO_2 (f = 2-4), if (1) added greenhouse gases are responsible for the temperature increase, (2) the 1850 CO_2 abundance was 270±10 ppm, and (3) the heat perturbation is mixed like a passive tracer in the ocean. This technique inherently yields a broad range for the inferred climate sensitivity, because the response time for the ocean increases with increasing climate sensitivity.

Thus the 3-D climate model, the 18K study and the empirical evidence from recent temperature trends yield generally consistent estimates of climate sensitivity. Our best estimate of the equilibrium climate sensitivity for processes occurring on the 10-100 year time scale is a global mean warming of 2.5-5°C for doubled CO_2.

Transient Climate Response

The rate at which the ocean surface can take up or release heat is limited by the fact that feedbacks come into play in conjunction with climate change, not in conjunction with climate forcing. Thus the (isolated) ocean mixed layer thermal relaxation time, commonly taken as 3-5 years, must be multiplied by the feedback factor f. This, in turn, allows the thermal inertia of deeper parts of the ocean to be effective. If the equilibrium climate sensitivity is ~4°C for doubled CO_2 and if small heat perturbations behave like observed passive tracers, the response time of surface temperature to a change of climate forcing is of order 100 years. If the equilibrium sensitivity is 2.5°C, this response time is about 40 years.

We conclude, based on the long surface temperature response time, that there is a large growing gap between current climate and the equilibrium climate for current atmospheric composition. Our projections indicate that within a few decades the equilibrium global temperature will reach a level well above that which has been experienced by modern man.

Is there a point at which the perturbation of surface climate will be large enough to substantially affect the rate of exchange of heat between the mixed layer and deeper ocean, possibly causing a rapid trend toward the equilibrium climate? This question is similar to one asked by Representative Gore (1982): "Is there a point where we trigger the dynamics of this (greenhouse) process, and if so, when do we reach that stage?". With present understanding of the climate system, particularly physical oceanography, we can not answer these questions.

Appendix A: Influence of Feedbacks on Transient Reponse

Consider a planet for which the absorbed fraction of incident solar radiation (1 minus albedo) is a linear function of the temperature, say x + yT. If the planet emits as a blackbody its temperature is determined by the condition of radiative equilibrium

$$s_o a_o = \sigma T_o^4 \qquad (A1)$$

with s_o the mean solar irradiance and $a_o = x+yT_o$.

Now suppose the solar irradiance changes suddenly by a small amount Δs. At the new equilibrium

$$(s_o + \Delta s)(a_o + \Delta a_{eq}) = \sigma(T_o + \Delta T_{eq})^4 \quad . \qquad (A2)$$

Neglecting second order terms (since $\Delta s << s_o$) and using (A1) yields

$$\Delta s a_o + s_o \Delta a_{eq} = 4\sigma T_o^3 \Delta T_{eq} \quad . \qquad (A3)$$

If there were no feedbacks ($\Delta a_{eq} = 0$), the temperature change at equilibrium would be

$$\Delta T_{eq}(\text{no feedbacks}) \equiv \Delta T_o = \frac{\Delta s a_o}{4\sigma T_o^3} \quad . \qquad (A4)$$

Thus we can rewrite (A3) as

$$\Delta T_{eq} = \Delta T_o + g\Delta T_{eq} \qquad (A5)$$

where

$$g = \frac{s_o \Delta a_{eq}}{4\sigma T_o^3 \Delta T_{eq}} = \frac{s_o y}{4\sigma T_o^3} \qquad (A6)$$

Using the relation between gain g and feedback factor f, f=1/(1-g), equation (A5) becomes

$$\Delta T_{eq} = f\Delta T_o \qquad (A7)$$

i.e., the equilibrium temperature change exceeds the no-feedback equilibrium temperature change by the factor f.

The heat flux into the planet as a function of time is

$$F = \Delta s a_o + s_o \Delta a - 4\sigma T_o^3 \Delta T$$

$$= 4\sigma T_o^3 (\Delta T_o + g\Delta T - \Delta T)$$

$$= \frac{4\sigma T_o^3 \Delta T_o}{\Delta T_{eq}} (\Delta T_{eq} - \Delta T)$$

$$= \frac{F_o}{\Delta T_{eq}} (\Delta T_{eq} - \Delta T) \qquad (A8)$$

where

$$F_o = 4\sigma T_o^3 \Delta T_o = \Delta s a_o \qquad (A9)$$

is the flux into the planet at t = 0 (i.e., when $\Delta T = 0$). Thus the initial rate of warming is independent of the feedbacks.

The temperature of the planet as a function of time is determined by the equation

$$\frac{dcT}{dt} = \frac{dc\Delta T}{dt} = F \qquad (A10)$$

where c is the heat capacity per unit area. If c is constant (e.g. a mixed layer without diffusion into deeper layers), the solution is

$$\Delta T = \Delta T_{eq}(1 - \exp(-t/\tau)), \qquad (A11)$$

$$\tau = f \frac{c}{4\sigma T_o^3} = f\tau_b \qquad (A12)$$

where τ_b is the no-feedback e-folding time [Equation (22)].

Finally, note that these results are much more general than the specific mechanism we chose for the feedback, which was only used as a concrete example. It is apparent from the above that the only assumption required is the linearization of the feedback as a function of temperature.

Acknowledgements. This work depended on essential scientific contributions from several people, in particular: K. Prentice applied the Koppen classification scheme to the control and 18K simulations, H. Brooks and L. Smith derived the 18K monthly sea surface temperatures and sea ice distributions from the February and August CLIMAP data, S. Lebedeff developed the chlorofluorocarbon scenarios, F. Abramopoulos performed calculations with the 1-D ocean model, D. Peteet provided advice and references on paleoclimate vegetation, and L.C. Tsang compiled mixed layer depths from ocean data tapes. We thank R.

Dickinson, L. Ornstein, W. Ruddiman, S. Schneider and C. Wunsch for critically reviewing the manuscript, J. Mendoza and L. DelValle for drafting the figures, and A. Calarco and C. Plamenco for typing several versions of the manuscript. Our climate model development was supported principally by the NASA Climate Program managed by Dr. Robert Schiffer; the applications to CO_2 studies were supported by a grant in 1982-1983 from EPA, for which we are indebted especially to John Hoffman, John Topping and Joseph Cannon.

References

Alexander, R.C., and R.L. Mobley, Monthly average sea-surface temperatures and ice-pack limits on a 1° global grid, Mon. Wea. Rev., 104, 143-148, 1976.

Berger, A.L., Long-term variations of daily insolation and quaternary climatic changes, J. Atmos. Sci., 35, 2362-2367, 1978.

Bode, H.W., Network Analysis and Feedback Amplifier Design, 551 pp., Van Nostrand, New York, 1945.

Broecker, W.S., T.H. Peng and R. Engh, Modeling the carbon system, Radiocarbon, 22, 565-598, 1980.

Bryan, K., F.G. Komro, S. Manabe and M.J. Spelman, Transient climate response to increasing atmospheric carbon dioxide, Science, 215, 56-58, 1982.

Bryan, K., F.G. Komro and C. Rooth, The ocean's transient response to global surface temperature anomalies, Maurice Ewing Series, 5, 1984.

Budyko, M.I., The effect of solar radiation variations on the climate of the earth, Tellus, 21, 611-619, 1969.

Burckle, L.H., D. Robinson and D. Cooke, Reappraisal of sea-ice distribution in Atlantic and Pacific sectors of the Southern Ocean at 18,000 yr BP, Nature, 299, 435-437, 1982.

CDAC, Changing Climate, Report of the Carbon Dioxide Assessment Committee, 496 pp., National Academy Press, Washington, D.C., 1983.

Cess, R.D., Radiative transfer due to atmospheric water vapor: global considerations of the earth's energy balance, J. Quant. Spectrosc. Radiat. Transfer, 14, 861-871, 1974.

Cess, R.D., Biosphere-albedo feedback and climate modeling, J. Atmos. Sci., 35, 1765-1769, 1978.

Cess, R.D. and S.D. Goldenberg, The effect of ocean heat capacity upon global warming due to increasing atmospheric carbon dioxide, J. Geophys. Res., 86, 498-502, 1981.

CLIMAP Project Members, A. McIntyre, project leader: Seasonal reconstruction of the earth's surface at the last glacial maximum, Geol. Soc. Amer., Map and Chart Series, No. 36, 1981.

Craig, H., and C.C. Chou, Methane: the record in polar ice cores, Geophys. Res. Lett., 9, 1221-1224, 1982.

Denton, G.H. and T.J. Hughes, The Last Great Ice Sheets, 484 pp., John Wiley, New York, 1981.

Dickinson, R.E., Vegetation albedo feedbacks, Maurice Ewing Series, 5, 1984.

DiLabio, R.N.W. and R.A. Klassen, Book review of The Last Great Ice Sheets, Bull. Amer. Meteorol. Soc., 64, 161, 1983.

Ehhalt, D.H., R.J. Zander and R.A. Lamontagne, On the temporal increase of tropospheric CH_4, J. Geophys. Res., 88, 8442-8446, 1983.

Flenley, J., The Equatorial Rain Forest: A Geological History, 162 pp., Butterworths, London, 1979.

Gates, W.L., Modeling the Ice-Age Climate, Science, 191, 1138-1144, 1976.

Gordon, A.L., Southern Ocean Atlas, 34 pp., 248 plates, Columbia Univ. Press, New York, 1982.

Gore, A., Record of Joint Hearing on Carbon Dioxide and Climate: The Greenhouse Effect, March 25, 1982, Science and Technology Committee (available from Goddard Institute for Space Studies, New York, 10025), 1982.

Hansen, J., D. Johnson, A. Lacis, S. Lebedeff, P. Lee, D. Rind and G. Russell, Climate impact of increasing atmospheric carbon dioxide, Science, 213, 957-966, 1981.

Hansen, J., D. Johnson, A. Lacis, S. Lebedeff, P. Lee, D. Rind and G. Russell, Climatic effects of atmospheric carbon dioxide, Science, 220, 873-875, 1983a.

Hansen, J., A. Lacis and S. Lebedeff, in Carbon Dioxide Review 1982, Oxford Univ. Press, New York, 284-289, 1982.

Hansen, J., A. Lacis, D. Rind and G. Russell, Climate sensitivity to increasing greenhouse gases, in Sea Level Rise to the Year 2100, Van Nostrand, New York, 1984.

Hansen, J., G. Russell, D. Rind, P. Stone, A Lacis, S. Lebedeff, R. Ruedy and L. Travis, Efficient three-dimensional global models for climate studies: models I and II, Mon. Wea. Rev., 111, 609-662, (paper 1), 1983b.

Hoffert, M.I., A.J. Callegari and C.T. Hsieh, The role of deep sea heat storage in the secular response to climatic forcing, J. Geophys. Res., 85, 6667-6679, 1980.

Hunt, B.G. and N.C. Wells, An assessment of the possible future climatic impact of carbon dioxide increases based on a coupled one-dimensional atmospheric-oceanic model, J. Geophys. Res., 84, 787-791, 1979.

Keeling, C.D., R.B., Bacastow and T.P. Whorf, in Carbon Dioxide Review 1982, ed. W.C. Clark, Oxford Univ. Press, New York, 377-385, 1982.

Kellogg, W.W. and S.H. Schneider, Climate stabilization: for better of worse?, Science, 1163-1172, 1974.

Koppen, W., Das geographische system der klimate, in Handbuch der Klimatologie 1, part C. ed. W. Koppen and G. Geiger, Boentraeger, Berlin, 1936.

Lacis, A., J. Hansen, P. Lee, T. Mitchell and S. Lebedeff, Greenhouse effect of trace gases, 1970-1980, Geophys. Res. Lett., 8, 1035-1038, 1981.

Levitus, S., Climatological Atlas of the World Ocean, NOAA Prof. Paper, No. 13, U.S. Government Printing Office, Washington, D.C., 1982.
Lian, M.S. and R.D. Cess, Energy-balance climate models: a reappraisal of ice-albedo feedback, J. Atmos. Sci., 34, 1058-1062, 1977.
Manabe, S., Carbon dioxide and climate change, Adv. Geophys., 25, 39-82, 1983.
Manabe, S. and D.G. Hahn, Simulation of the tropical climate of an ice age, J. Geophys. Res., 82, 3889-3911, 1977.
Manabe, S., J. Smagorinsky and R.F. Strickler, Simulated climatology of a general circulation model with a hydrologic cycle, Mon. Wea. Rev., 98, 175-212, 1965.
Manabe, S. and R.J. Stouffer, Sensitivity of a global climate model to an increase of CO_2 concentration in the atmosphere, J. Geophys. Res., 85, 5529-5554, 1980.
Manabe, S. and R.T. Wetherald, Thermal equilibrium of the atmosphere with a given distribution of relative humidity, J. Atmos. Sci., 24, 241-259, 1967.
Manabe, S. and R.T. Wetherald, The effects of doubling the CO_2 concentration on the climate of a general circulation model, J. Atmos. Sci., 32, 3-15, 1975.
Manabe, S. and R.T. Wetherald, On the distribution of climate change resulting from an increase of CO_2 content of the atmosphere, J. Atmos. Sci., 37, 99-118, 1980.
Matthews, E., Global vegetation and land use: new high-resolution data bases for climate studies, J. Clim. Appl. Meteorol., 22, 474-487, 1983.
Miller, J.R., G.L. Russell and L.C. Tsang, Annual oceanic heat transports computed from an atmospheric model, Dynam. Atmos. Oceans, 7, 95-109, 1983.
NAS, Understanding Climatic Change, 239 pp., National Academy of Sciences, Washington, D.C., 1975.
Neftel, A., H. Oeschger, J. Swander, B. Stauffer and R. Zumbrunn, Ice core sample measurements give atmospheric CO_2 content during the past 40,000 years, Nature, 295, 220-223, 1982.
NOAA, User's Guide to NODC Data Services, Environmental Data Service, Washington, D.C., 1974.
North, G.R., Theory of energy-balance climate models, J. Atmos. Sci., 32, 2033-2043, 1975.
Ostlund, H.G., H.G. Dorsey and R. Brescher, GEOSECS Atlantic radiocarbon and tritium results, Univ. Miami Tritium Laboratory Data Report No. 5, 1976.
Robock, A., The dust cloud of the century, Nature, 301, 373-374, 1983.
Sarnthein, M., Sand deserts during glacial maximum and climatic optimum, Nature, 272, 43-46, 1978.
Schneider, S.H. and S.L. Thompson, Atmospheric CO_2 and climate: importance of the transient response, J. Geophys. Res., 86, 3135-3147, 1981.
Sellers, W.D., A global climate model based on the energy balance of the earth-atmosphere system, J. Appl. Meteorol., 8, 392-400, 1969.
Shackleton, N.J., M.A. Hall, J. Line and C. Shuxi, Carbon isotope data in core V19-30 confirm reduced carbon dioxide concentration in the ice age atmosphere, Nature, 306, 319-322, 1983.
Street, F. and A. Grove, Global maps of lake-level fluctuations since 30,000 yr BP, Quat. Res., 12, 83-118, 1979.
Stone, P.H., Feedbacks between dynamical heat fluxes and temperature structure in the atmosphere, Maurice Ewing Series, 5, 1984.
Vuilleumier, B., Pleistocene changes in the fauna and flora of South America, Science, 173, 771 780, 1971.
Walsh, J. and C. Johnson, An analysis of Arctic sea ice fluctuations, J. Phys. Ocean., 9, 580-591, 1979.
Wang, W.C. and P.H. Stone, Effect of ice-albedo feedback on global sensitivity in a one-dimensional radiative-convective climate model, J. Atmos. Sci., 37, 545-552, 1980.
Webster, P.J. and N.A. Streten, Late Quaternary ice age climates of tropical Australia: interpretations and reconstructions, Quat. Res., 10, 279-309, 1978.
Weiss, R.F., The temporal and spatial distribution of tropospheric nitrous oxide, J. Geophys. Res., 86, 7185-7195, 1981.
Wetherald, R.T. and S. Manabe, The effects of changing the solar constant on the climate of a general circulation model, J. Atmos. Sci., 32, 2044-2059, 1975.
Williams, J., R.G. Barry and W.M. Washington, Simulation of the atmospheric circulation using the NCAR global circulation model with ice age boundary conditions, J. Appl. Meteorol., 13, 305-317, 1974.
WMO, World Meteorological Organization project on research and monitoring of atmospheric CO_2, Report no. 10, R.J. Bojkov ed., Geneva, 42 pp., 1983.